# DYNAMIC MODELING AND FEEDBACK CONTROL WITH MODE-SHIFTING OF A TWO-MODE ELECTRICALLY VARIABLE TRANSMISSION

A Thesis
Presented to
The Academic Faculty

by

Ashish S. Katariya

In Partial Fulfillment
of the Requirements for the Degree
Master of Science in the
School of Electrical and Computer Engineering

Georgia Institute of Technology
December 2012

# DYNAMIC MODELING AND FEEDBACK CONTROL WITH MODE-SHIFTING OF A TWO-MODE ELECTRICALLY VARIABLE TRANSMISSION

Approved by:

Professor David G. Taylor,
Committee Chair
School of Electrical and Computer Engineering
*Georgia Institute of Technology*

Professor Magnus B. Egerstedt
School of Electrical and Computer Engineering
*Georgia Institute of Technology*

Professor Michael J. Leamy
School of Mechanical Engineering
*Georgia Institute of Technology*

Date Approved: 24 August, 2012

*This thesis is dedicated to my family for their love and support.*

# ACKNOWLEDGEMENTS

First and foremost I owe my deepest gratitude and regard to my advisor and mentor, Prof. David G. Taylor for mentoring me and supporting me throughout my graduate degree. I would like to thank him for his immense help and patience as I completed the thesis. This thesis would not have been possible unless it was for his motivation, enthusiasm and knowledge of the subject matter. Besides my advisor, I would like to thank Professors Michael J. Leamy and Magnus B. Egerstedt for agreeing to be a part of my thesis committee and providing valuable feedback.

I would also like to acknowledge support from the Department of Energy under Award Number DE-EE0002627 and from the EcoCAR Challenge, a three-year collegiate advanced vehicle technology engineering competition established by the Department of Energy and General Motors, and managed by Argonne National Laboratory.

Last but not the least, I am grateful to my parents for encouraging me throughout my life and supporting me while I completed this thesis.

# TABLE OF CONTENTS

# LIST OF TABLES

# LIST OF FIGURES

# SUMMARY

This thesis develops dynamic models for the two-mode FWD EVT, develops a control system based on those models that is capable of meeting driver torque demands and performing synchronous mode shifts between different EVT modes while also accommodating preferred engine operating points. The two-input two-output transmission controller proposed herein incorporates motor-generator dynamics, is based on a general state-space integral control structure, and has feedback gains determined using linear quadratic regulator (LQR) optimization.

Dynamic modeling of the vehicle is categorized as dynamic modeling of the mechanical and electrical subsystems where the mechanical subsystem consists of the planetary gear sets, the transmission and the engine whereas the electrical subsystem consists of the motor-generator units and the battery pack. A discussion of load torque is also considered as part of the mechanical subsystem. With the help of these derived dynamic models, a distinction is made between dynamic output torque and steady-state output torque.

The overall control system consisting of multiple subsystems such as the human driver, power management unit (PMU), friction brakes, combustion engine, transmission control unit (TCU) and motor-generator units is designed. The logic for synchronous mode shifts between different EVT modes is also detailed as part of the control system design. Finally, the thesis presents results for responses in individual operating modes, EVT mode shifting and a full UDDS drive cycle simulation.

# CHAPTER I

# INTRODUCTION

## *1.1 Background*

As a result of increasing concerns over limited fossil fuels and related environmental impacts, hybrid electric vehicles (HEVs) have attracted a great deal of attention in the automotive industry. Various HEV architectures have been introduced over the last 15 years. Traditionally, HEVs have been categorized into three types, namely the series architecture, parallel architecture and power-split architecture [1]. Although the engine operates independently and unlimited transmission speed ratios are available in the series architecture, the size of large electric machines makes it infeasible for certain vehicle types. Alternatively, the parallel architecture costs less and provides higher transmission efficiency but relies heavily on the engine and gasoline fuel. The power-split architecture uses power-split gearing to split power into two paths (all-mechanical and electro-mechanical) and thus combines benefits of the series and parallel architectures [2].

For instance, Toyota Prius, the best-selling HEV in the world implements a power-split architecture. An electrically variable transmission (EVT) is a type of power-split transmission. It makes use of two motor-generator units to electrically impose a continuously variable ratio between the engine crankshaft and the transmission drive shaft, thereby permitting the engine to supply power in a thermally-efficient manner irrespective of vehicle speed; it achieves this type of operation by diverting an electrically controlled amount of engine power away from the direct mechanical path to the wheels. The EVT used in Toyota Prius is called a one-mode EVT because it has one planetary gear set and provides one mechanical point.

However, since the one-mode EVT uses high electro-mechanical power with higher engine speeds, and electro-mechanical power is less efficient, General Motors (GM) invented the two-mode EVT with two (or three) planetary gear sets [3]. Usage of an extra mechanical point in two-mode EVT limits electro-mechanical power for acceleration, hills and towing. Thus, two-mode EVTs maintain high efficiency over a wider range of speed ratios and transmit more power mechanically. The first two-mode EVT architecture introduced by GM consisted of three simple planetary gear sets. Due to the number of components along the transmission and sizing constraints, usage of two-mode EVT was restricted to trucks and other large vehicles that were often rear-wheel-drive (RWD) in nature [4]. As a result, most of the modeling and control system development for two-mode EVT was done for the RWD architecture [5], [6].

Recently, a new two-mode EVT architecture for front-wheel-drive (FWD) applications was invented by GM and it is described in [4]. The two-mode FWD EVT architecture consists of two planetary gear sets (one compound and one simple) compared to three in the RWD architecture. This new architecture can thus be packaged into the basic space constraints of a conventional automatic transmission [4]. Since the two-mode FWD EVT is an advanced hybrid architecture available for mid-size sedans today, its modeling and control becomes an important subject area. Additionally, two-mode EVTs can be operated with engine mechanically independent from the final drive shaft or in various mechanical/electrical split contributions thus enabling multi-mode operation, electrically assisted launches, regenerative braking and engine off idling [7]. The purpose of this thesis is to develop dynamic models for the two-mode EVT of [4], and to further develop a control system based on those models that is capable of meeting driver torque demands and performing synchronous mode shifts between different EVT modes while also accommodating preferred engine operating points.

## *1.2 Literature Review*

Control system development for HEVs can be viewed at multiple levels of abstraction. At the higher level, a power management unit (PMU) or supervisory controller ensures that for a given driver's request of output torque, the vehicle is at its most efficient operating point. This is done by managing power among vehicle components such as the engine and battery [8]. The PMU thus dictates the operating point (speed and torque) of the engine at any given instant of time. Whereas, at the lower level, the transmission control unit (TCU) accepts reference commands from the PMU and produces torque commands for the motors/generators. Modeling of low-level transmission dynamics in state-space form is critical for the development of an effective transmission control unit. This modeling effort and control system development for two-mode FWD EVT has received little attention in the research community.

The same two-mode FWD EVT described in [4] is considered in [9] and [10], but dynamic modeling is not pursued. The dynamic models of two particular EVTs are reported in [8] and [11], but the associated transmission controllers are not disclosed. Also, most control system development in this area has been done for the PMU [5], [12]. In such works, low-level transmission dynamics have usually been accounted for using Simulink models or the Powertrain System Analysis Toolkit (PSAT) [2], [5], [13], [14]. While such methods are convenient for simulation purposes, they don't fully reveal the internal transmission dynamics.

Some modeling and simulation efforts apply a backward-looking approach which is a good predictor of vehicle performance, energy usage and mileage, but it can be applied only to specific drive cycles wherein prior knowledge of vehicle speed is assumed to be known [15]. Note that backward-looking simulations do not account for driver's behavior and use a steady-state approach. Therefore, such an approach cannot be used for traditional control system development that accounts for all dynamics and transients [15].

The transmission controller for a single-mode EVT is reported in [2], but perfect torque sources are assumed and a decoupling type of proportional-integral control is suggested. In contrast, the transmission controller proposed herein incorporates motor-generator dynamics, is based on a general state-space integral control structure, and has feedback gains determined using linear quadratic regulator (LQR) optimization. Also, this thesis presents an EVT mode shifting control strategy while using and extending the transmission controller presented in [16].

## *1.3 Thesis Outline*

As mentioned earlier, the objective of this thesis is to develop dynamic models for the two-mode FWD EVT, and to further develop a control system based on those models that is capable of meeting driver torque demands and performing synchronous mode shifts between different EVT modes while also accommodating preferred engine operating points. Hence, dynamic modeling of the vehicle will be described first, followed by the overall control system design, and eventually the simulation results will be presented.

Dynamic modeling of the vehicle will be categorized as dynamic modeling of the mechanical and electrical subsystems where the mechanical subsystem consists of the planetary gear sets, the transmission and the engine whereas the electrical subsystem consists of the motor-generator units and the battery pack. A discussion of load torque will also be considered as part of the mechanical subsystem. Now, before the overall control system will be described, a detailed analysis of output torque capability for a given powertrain design at various vehicle speeds will be presented because it is important to check whether or not a given powertrain design is capable of meeting desired performance requirements.

Following the analysis of output torque, the overall control system consisting of multiple subsystems such as the human driver, the power management unit (PMU),

the friction brakes, the combustion engine, the transmission control unit (TCU), and the motor-generator units will be described. The logic for synchronous mode shifts between different EVT modes will also be detailed as part of the control system design. Finally, the thesis will present results for responses in individual operating modes, EVT mode shifting and a full UDDS drive cycle simulation.

# CHAPTER II

# DYNAMIC MODELING OF TWO-MODE EVT

The stick diagram of the two-mode FWD EVT considered in this thesis is shown in Figure 1. The engine port and the output port are identified by the inward and outward arrows, respectively. The planetary gear set at the engine port, labeled $PG_1$, has a double layer of planets, whereas the planetary gear set at the output port, labeled $PG_2$, has a single layer of planets. Various operating modes are activated according to the state of the clutches, labeled $C_1$, $C_2$, $C_3$ and $C_4$, and the state of the engine, as indicated in Table 1.

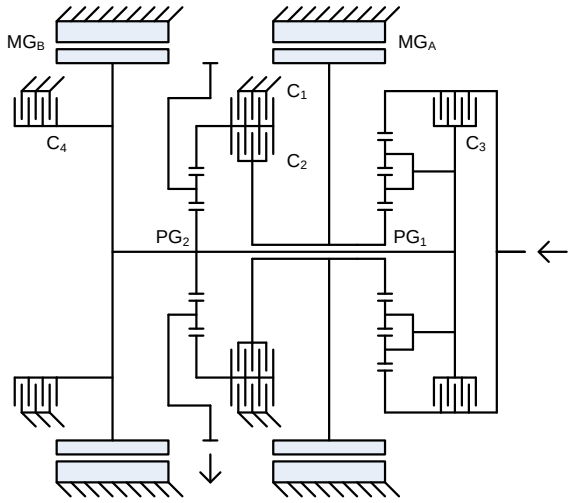


**Figure 1:** Stick diagram of two-mode EVT.

The first EVT mode, referred to as EVT-1, is activated by engaging only clutch $C_1$. The second EVT mode, referred to as EVT-2, is activated by engaging only clutch $C_2$. In both EVT modes, the motor-generator units are used to impose a continuously variable ratio between the engine port and the output port. Special cases of the EVT modes, referred to as Electric-1 and Electric-2, exploit the continuously variable ratio

**Table 1:** Operating Modes of the EVT

| Mode | $C_1$ | $C_2$ | $C_3$ | $C_4$ | Engine |
|---|---|---|---|---|---|
| Electric-1 | × | | | | off |
| Electric-2 | | × | | | off |
| EVT-1 | × | | | | on |
| EVT-2 | | × | | | on |
| FG-1 | × | | × | | on |
| FG-2 | × | × | | | on |
| FG-3 | | × | × | | on |
| FG-4 | | × | | × | on |

property to permit engine-off operation with engine speed equal to zero. In addition to the two EVT modes, four fixed gear modes are also available; in these operating modes, the ratio between the engine port and the output port is not variable. Fixed gear modes are not considered here.

## *2.1 Mechanical Subsystem*

In either of the EVT modes, the transmission is considered to contain four primary rigid bodies that may rotate about a central axis. These bodies will be referred to as the engine body $e$, the output body $o$, and the electric machine bodies $a$ and $b$. Since the transmission is externally connected at its engine port and output port, bodies $e$ and $o$ are defined so as to account for those external connections. The four rotational bodies are characterized by their speeds $\omega_e$, $\omega_o$, $\omega_a$ and $\omega_b$ and their inertias $I_e$, $I_o$, $I_a$ and $I_b$.

To simplify the modeling, the mass of each planet gear associated with a planetary gear set is assumed to be concentrated at its axis of rotation; hence, although the mass of each planet gear contributes to the inertia of the carrier, each planet gear has zero inertia with respect to its own rotation axis.

### 2.1.1 Planetary Gear Sets and Kinematics

The planetary gear sets introduce kinematic constraints, so there are just two independent speeds. Choosing $\omega_e$ and $\omega_o$ as the independent speeds, the kinematic constraints for the electric machines may be expressed in the form

$$\begin{bmatrix} \omega_a \\ \omega_b \end{bmatrix} = \begin{bmatrix} \gamma_{ae} & \gamma_{ao} \\ \gamma_{be} & \gamma_{bo} \end{bmatrix} \begin{bmatrix} \omega_e \\ \omega_o \end{bmatrix} \tag{1}$$

and the kinematic constraint defining the bearing speed of any given planet gear may be similarly written in the form

$$\omega_p = \gamma_{pe}\omega_e + \gamma_{po}\omega_o. \tag{2}$$

The bearing speed of each planet gear must be restricted to a limited speed range specified according to

$$|\omega_p| \leq \omega_p^{\max}.$$

All the $\gamma$ values are dimensionless ratios that depend on which operating mode has been selected.

The $\gamma$ values associated with the electric machines shown in (1) are mode dependent; they may be expressed in terms of the characteristic ratios of the planetary gear sets defined by

$$\rho_i = \frac{\text{number of sun gear teeth on PG}_i}{\text{number of ring gear teeth on PG}_i}, \quad i = 1, 2.$$

For EVT-1 they are

$$\begin{bmatrix} \gamma_{ae} & \gamma_{ao} \\ \gamma_{be} & \gamma_{bo} \end{bmatrix}_1 = \frac{1}{\rho_1\rho_2} \begin{bmatrix} \rho_2 & -(1-\rho_1)(1+\rho_2) \\ 0 & \rho_1(1+\rho_2) \end{bmatrix}. \tag{3}$$

For EVT-2 they are

$$\begin{bmatrix} \gamma_{ae} & \gamma_{ao} \\ \gamma_{be} & \gamma_{bo} \end{bmatrix}_2 = \frac{1}{1-\rho_1-\rho_1\rho_2} \begin{bmatrix} -\rho_2 & (1-\rho_1)(1+\rho_2) \\ 1 & -\rho_1(1+\rho_2) \end{bmatrix}. \tag{4}$$

The $\gamma$ values associated with the internal planet gears shown in (2) are mode dependent, due to the fact that planetary gear set external speeds are related to independent speeds in a mode-dependent fashion. Rather than stating their values explicitly, it is more convenient to define these $\gamma$ values implicitly given that

$$\text{PG}_1 \text{ inner-planet bearing speed} = \frac{n_{s1}}{n_{p1i}} (\omega_b - \omega_a)$$

$$\text{PG}_1 \text{ outer-planet bearing speed} = \frac{n_{r1}}{n_{p1o}} (\omega_e - \omega_b)$$

$$\text{PG}_2 \text{ planet bearing speed} = \frac{n_{s2}}{n_{p2}} (\omega_o - \omega_b)$$

where $n_x$ denotes the number of teeth on gear $x$. Note that the $(\gamma_{pe}, \gamma_{po})$ parameters change with mode, since the relationship between $(\omega_a, \omega_b)$ and $(\omega_e, \omega_o)$ changes with mode.

The kinematic relations given in (1) will now be used to derive the differential equations that model transmission dynamics for a two-mode EVT.

### 2.1.2 Transmission Dynamics

The dynamic equations may be obtained by conservation of energy principles. Neglecting internal friction losses, and assuming that the positive direction of power flow is into ports $e$, $a$ and $b$, but out of port $o$, the resulting power balance is

$$T_e\omega_e - T_l\omega_o + T_a\omega_a + T_b\omega_b = I_e\omega_e\dot{\omega}_e + I_o\omega_o\dot{\omega}_o + I_a\omega_a\dot{\omega}_a + I_b\omega_b\dot{\omega}_b \tag{5}$$

where $T_e$, $T_l$, $T_a$ and $T_b$ refer to engine torque, load torque and electric machine torques, respectively. Recall that $\omega_e$ and $\omega_o$ were chosen as independent speeds. Applying the kinematic constraints given in (1), the power balance equation can be rewritten as the coupled differential equations

$$\gamma_{ae}T_a + \gamma_{be}T_b + T_e = I_e\dot{\omega}_e + I_a\gamma_{ae}(\gamma_{ae}\dot{\omega}_e + \gamma_{ao}\dot{\omega}_o) + I_b\gamma_{be}(\gamma_{be}\dot{\omega}_e + \gamma_{bo}\dot{\omega}_o) \tag{6}$$

$$\gamma_{ao}T_a + \gamma_{bo}T_b - T_l = I_o\dot{\omega}_o + I_a\gamma_{ao}(\gamma_{ae}\dot{\omega}_e + \gamma_{ao}\dot{\omega}_o) + I_b\gamma_{bo}(\gamma_{be}\dot{\omega}_e + \gamma_{bo}\dot{\omega}_o). \tag{7}$$

Rearranging the above equations, we have

$$\begin{bmatrix} J_{ee} & J_{eo} \\ J_{eo} & J_{oo} \end{bmatrix} \begin{bmatrix} \dot{\omega}_e \\ \dot{\omega}_o \end{bmatrix} = \begin{bmatrix} \gamma_{ae} T_a + \gamma_{be} T_b + T_e \\ \gamma_{ao} T_a + \gamma_{bo} T_b - T_l \end{bmatrix} \tag{8}$$

where the inertia values are given by

$$\begin{aligned} J_{ee} &= I_e + \gamma_{ae}^2 I_a + \gamma_{be}^2 I_b \\ J_{eo} &= \gamma_{ae}\gamma_{ao} I_a + \gamma_{be}\gamma_{bo} I_b \\ J_{oo} &= I_o + \gamma_{ao}^2 I_a + \gamma_{bo}^2 I_b. \end{aligned}$$

Note that the coefficients parameterizing the dynamic equations are mode dependent.

### 2.1.3 Road Load

The load torque is simply the road load reflected to the output port of the transmission. For a level road with no wind, the load torque is given by

$$T_l = \rho_f r_w \left( c_r m_v g + \tfrac{1}{2} \varrho_a a_f c_d (\rho_f r_w \omega_o)^2 \right) \operatorname{sgn}(\omega_o) \tag{9}$$

where $\rho_f$ is the final drive ratio, $r_w$ is the wheel radius, $c_r$ is the rolling resistance coefficient, $m_v$ is the vehicle mass, $g$ is the acceleration of gravity, $\varrho_a$ is the density of air, $a_f$ is the frontal area, and $c_d$ is the aerodynamic drag coefficient.

### 2.1.4 Engine

The engine is a torque-controlled component, so its torque $T_e$ is governed by the differential equation

$$\dot{T}_e = \left( T_e^* - T_e \right) / \tau_e \tag{10}$$

where $T_e^*$ denotes the torque command and $\tau_e$ denotes the time constant. The torque command is restricted by

$$0 \leq T_e^* \leq T_e^{\max}.$$

The bound on the torque command is speed dependent and, in particular, it is nonzero only on the limited speed range

$$\omega_e^{\min} \leq \omega_e \leq \omega_e^{\max}.$$

Various portions of the powertrain control system are responsible for imposing these operational bounds.

## *2.2 Electrical Subsystem*

When in an electric mode or EVT mode, the transmission is controlled by electric machines under the influence of power converter circuits; the combination of an electric machine, its power converter circuit and its associated control algorithm is referred to as a motor-generator unit. For the purposes of this study, a detailed description of the motor-generator units is not necessary; only their overall operation is considered.

### 2.2.1 Motor-Generator Units

Each motor-generator unit is a torque-controlled component, so its torque $T_i$ is governed by the differential equation

$$\dot{T}_i = \left(T_i^* - T_i\right)/\tau_i, \quad i = a, b \tag{11}$$

where $T_i^*$ denotes the torque command and $\tau_i$ denotes the time constant. The torque command is restricted so as to satisfy the lower-speed torque constraint

$$|T_i^*| \leq T_i^{\max}$$

and the higher-speed power constraint

$$|T_i^* \omega_i| \leq P_i^{\max}.$$

These bounds on the torque command depend directly on speed and indirectly on bus voltage; they are nonzero only on the limited speed range

$$|\omega_i| \leq \omega_i^{\max}.$$

Various portions of the powertrain control system are responsible for imposing these operational bounds.

### 2.2.2 Battery Pack

A Thevenin equivalent circuit is used to represent the battery pack, with constant open-circuit voltage $V_s$, constant internal resistance $R_s$, and constant ideal charge capacity $Q_s$. The battery pack state of charge $q_s$ is governed by the differential equation

$$\dot{q}_s = -\frac{V_s - \sqrt{V_s^2 - 4R_s p_l}}{2R_s Q_s} \tag{12}$$

where $p_l$ is the electric power delivered to all loads. If the only loads are the motor-generator units, then

$$p_l = \frac{T_a \omega_a}{\eta_a} + \frac{T_b \omega_b}{\eta_b} \tag{13}$$

where $\eta_a$ and $\eta_b$ are the power conversion efficiencies.

# CHAPTER III

# CONTROL SYSTEM DESIGN

Before a control system can be successfully designed and simulated, it is important to check whether or not a given powertrain design is capable of meeting desired performance requirements. To this extent, the next section will provide an analysis of output torque capability and requirement for a given powertrain design at various vehicle speeds. Section 3.2 will then give details of the overall control system.

## *3.1 Analysis of Output Torque*

The existing literature is unclear on certain issues related to the interpretation of EVT output torque, so this analysis section is intended to clarify this important subject.

### 3.1.1 Torque Equilibrium Conditions

Most EVT analyses appearing in the literature have been based on steady-state modeling concepts. Dynamic models describe the relationships between torques and accelerations and, consequently, these models also describe the equilibrium conditions under which all speeds are constant. From the dynamic model presented in (8), equilibrium requires that the various torques be algebraically related according to

$$\gamma_{ae}\bar{T}_a + \gamma_{be}\bar{T}_b + \bar{T}_e = 0$$

$$\gamma_{ao}\bar{T}_a + \gamma_{bo}\bar{T}_b - \bar{T}_l = 0.$$

The bar notation is used to imply that these equilibrium torques are constant, rather than time-varying. From these equations, it is clear that the equilibrium value of

output torque, which will be denoted by $\bar{T}_o$, must be equal to

$$\bar{T}_o = \gamma_{ao}\bar{T}_a + \gamma_{bo}\bar{T}_b$$

since only then would the output torque and the load torque be equal and opposite as required to maintain constant output speed. It would be incorrect to infer that this same expression for output torque—rewritten without the bar notation—also holds true in non-equilibrium conditions.

### 3.1.2 Output Torque Definition

The most logical way to define output torque would be to identify the torque that determines acceleration at the output port. The mechanical dynamic equation involves coupling due to the non-diagonal inertia matrix, so the accelerating components of torque can only be isolated by further algebraic manipulation. For the output port, the differential equation resulting from such manipulation has the simplified form

$$J_o\dot{\omega}_o = T_o - T_l \tag{14}$$

where $T_o$ denotes the output torque defined by

$$T_o = \gamma_a T_a + \gamma_b T_b + \gamma_e T_e, \tag{15}$$

the dimensionless output torque coefficients are

$$\gamma_a = \gamma_{ao} - \frac{J_{eo}}{J_{ee}}\gamma_{ae}$$
$$\gamma_b = \gamma_{bo} - \frac{J_{eo}}{J_{ee}}\gamma_{be}$$
$$\gamma_e = -\frac{J_{eo}}{J_{ee}}$$

and the effective output inertia is

$$J_o = J_{oo} - \frac{J_{eo}}{J_{ee}}J_{eo}.$$

Note that $T_o \neq \gamma_{ao} T_a + \gamma_{bo} T_b$ except for the special case where all speeds are constant. $T_o$ contains additional terms not present in $\gamma_{ao} T_a + \gamma_{bo} T_b$, and their sum is nonzero during periods of acceleration.

### 3.1.3 Output Torque Capability

It is of interest to determine the limits on achievable output torque, as a function of vehicle speed, for various fixed engine operating states pre-selected on the basis of thermal efficiency considerations. Such information would be needed to check whether or not a given powertrain design meets performance requirements. To evaluate such output torque limits, at any given vehicle speed, consider the optimization problem

$$\begin{aligned} \text{maximize} \quad & |T_o| = |\gamma_a T_a + \gamma_b T_b + \gamma_e T_e| \\ \text{subject to} \quad & T_e = T_e^* \text{ and } \omega_e = \omega_e^* \\ & T_a \text{ and } T_b \text{ are within specified limits} \\ & \text{all speeds are within specified limits} \end{aligned}$$

where $(T_e^*, \omega_e^*)$ denotes a desired engine operating state; battery power limits are not considered here. The goal is to find the optimizing $T_a$ and $T_b$, if a solution exists, for each desired vehicle speed and for a given mode of operation. It is worth pointing out that if this optimization problem were modified to maximize $|\gamma_{ao} T_a + \gamma_{bo} T_b|$ rather than $|T_o|$, the result would be an over-estimation of powertrain performance.

### 3.1.4 Output Torque Requirement

The analysis that led to the definition of output torque also serves to clarify output torque requirements. The differential equation describing acceleration at the output port may be rewritten in the form

$$T_o = T_l + J_o \dot{\omega}_o.$$

If a drive cycle is specified, then corresponding required time-trajectories for $\omega_o$ and $\dot{\omega}_o$ are known, so the above equation may be evaluated to determine the corresponding

required time-trajectory for $T_o$. Clearly, this drive cycle requirement on $T_o$ must not exceed the achievable $T_o$ as determined in Section 3.1.3. Note that the effective output inertia $J_o$ is larger than $m_v(\rho_f r_w)^2$, the component due to vehicle mass in translation; moreover, since $J_o$ is mode dependent, the so-called mass factor of an EVT is as well.

### 3.1.5 Torque Capability in Operating Modes

The previous sections discussed how output torque capability and requirement can be calculated for a given powertrain design and drive cycle. It is now desirable to compare the output torque capability and requirement to determine if the powertrain design is capable of meeting performance requirements and thus following the drive cycle. All vehicle parameter values are specified in Table 3, the assumed drive cycle is UDDS and all Matlab code for generating the plots shown in this chapter is provided in Appendix A.

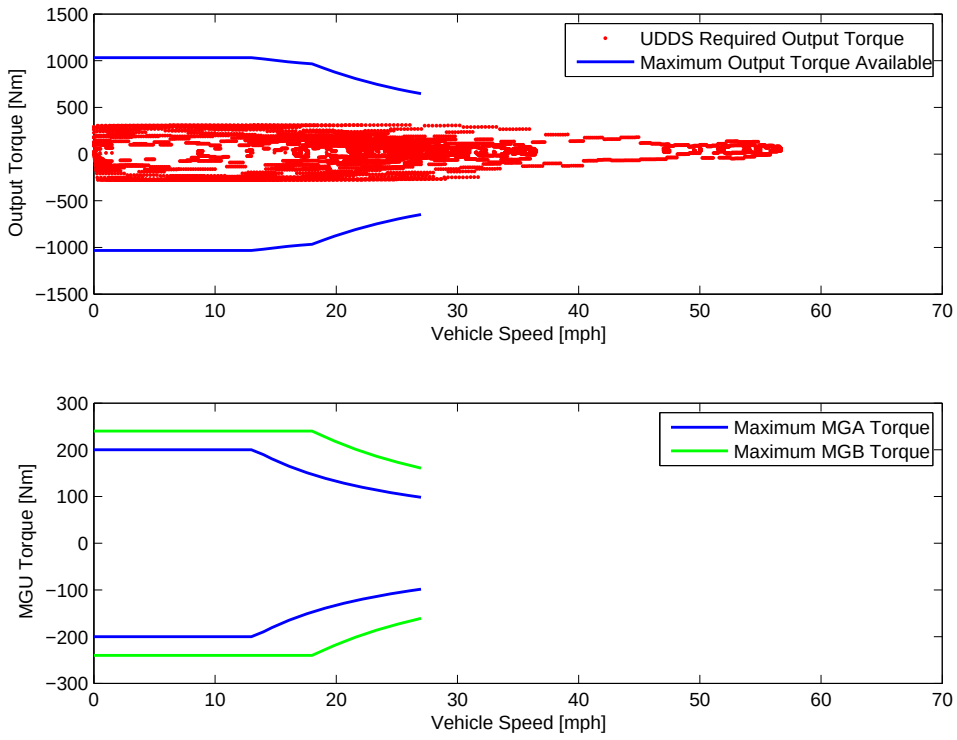


**Figure 2:** Torque capability in Electric-1.

The maximum output torques available in modes Electric-1 and Electric-2, along

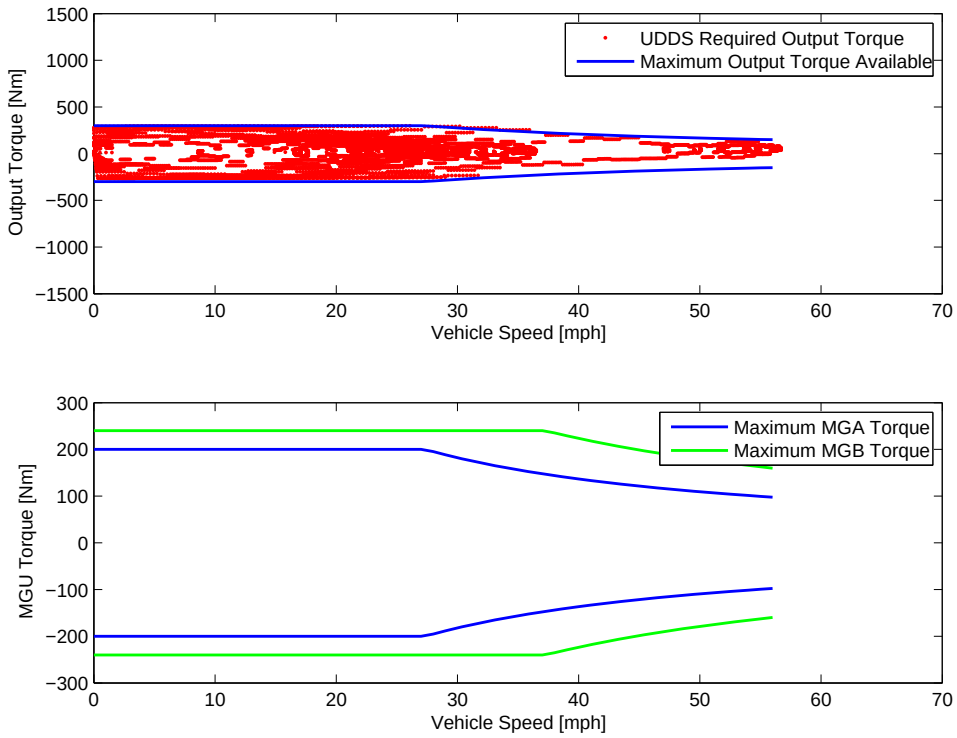


**Figure 3:** Torque capability in Electric-2.

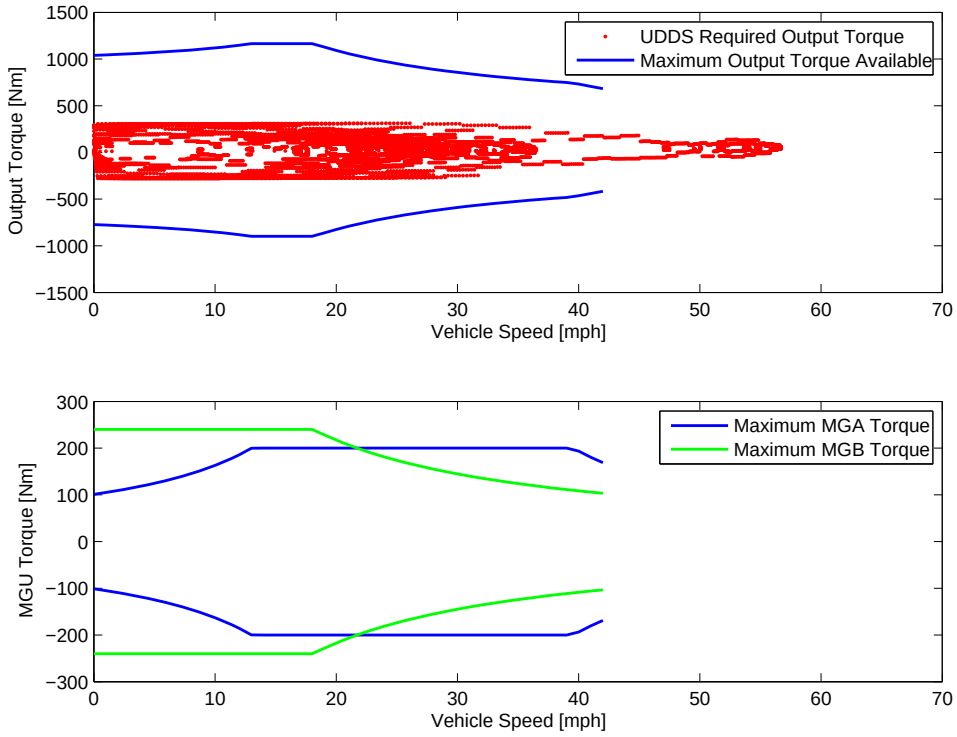


**Figure 4:** Torque capability in EVT-1; $T_e = 100$ Nm, $\omega_e = 2000$ rpm.

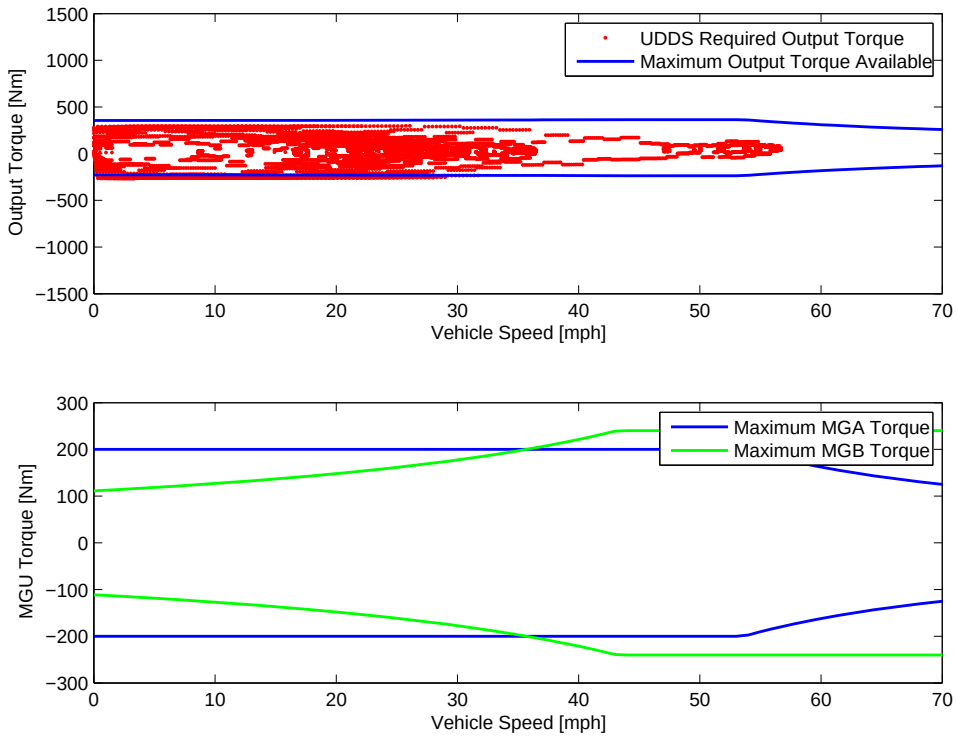


**Figure 5:** Torque capability in EVT-2; $T_e = 100$ Nm, $\omega_e = 2000$ rpm.

with the UDDS required output torques, are shown in Figures 2 and 3, respectively. The Electric-1 mode is restricted to low vehicle speed due to the limitation on planet gear bearing speed. The Electric-2 mode is not feasible, since the required torques are at the capability limits for high speeds and low speeds.

The maximum output torques available in modes EVT-1 and EVT-2 for $T_e = 100$ Nm and $\omega_e = 2000$ rpm, along with the UDDS required output torques, are shown in Figures 4 and 5, respectively. Note that for low vehicle speeds in EVT-2, the required torques are outside the capability limits but for high speeds, the required torques are well within the capability limits. This reinforces the well-known fact that EVT-1 is feasible for low vehicle speeds only and EVT-2 is feasible for high vehicle speeds. Thus, even though neither of these modes can meet all the requirements individually, the combination of these modes would do so easily, suggesting the need to switch modes at some intermediate speed.

## *3.2 Control System*

The overall control system consists of multiple subsystems, including the human driver, the power management unit (PMU), the friction brakes, the combustion engine, the transmission control unit (TCU), and the motor-generator units. The various reference commands involved are summarized in Table 2 and a block diagram of the overall control system is shown in Figure 6.

**Table 2:** Reference Commands

| Signal | Origin | Destination |
|---|---|---|
| $\omega_o^*$ | Driver | Driver |
| $T_o^*$ | Driver | PMU |
| $T_f^*$ | PMU | Brakes |
| $T_e^*$ | PMU | Engine |
| $M^*$ | PMU | TCU |
| $T_c^*$ | PMU | TCU |
| $\omega_e^*$ | PMU | TCU |
| $T_a^*$ | TCU | MGA |
| $T_b^*$ | TCU | MGB |

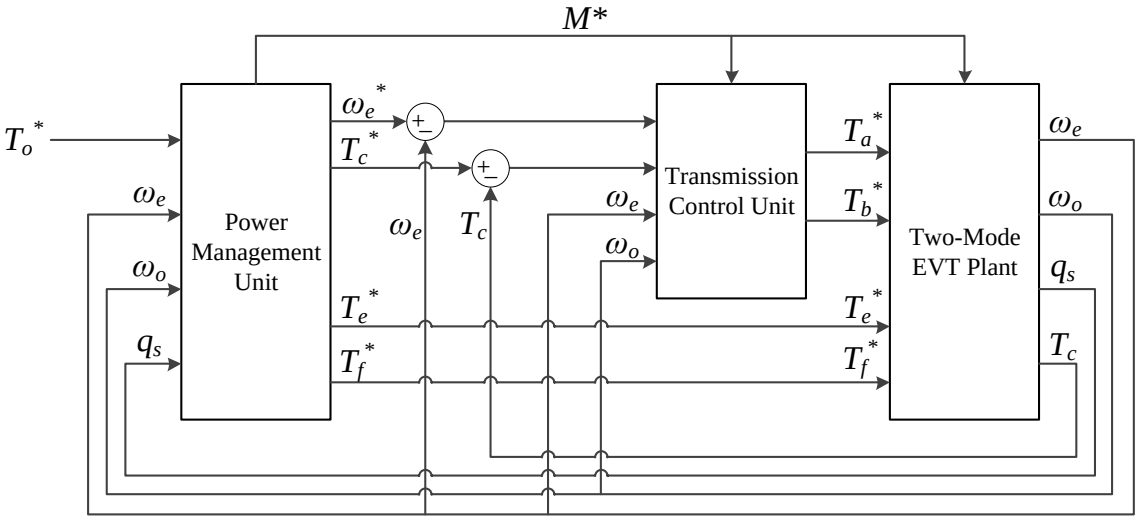


**Figure 6:** Overall control system block diagram.

Note that in the block diagram shown in Figure 6, the motor-generator units, the engine and the friction brakes are represented as part of the Two-Mode EVT Plant,

and the human driver control loop is excluded from the block diagram. Representing the block diagram in this fashion places emphasis on the PMU and TCU. Elaborate torque-control of the engine and motor-generator units is not the main focus of this study. For purposes of simulation, as mentioned earlier, these torque-controlled components are governed according to (10) and (11). The following sections will define and explain the purpose of each subsystem and reference command shown in Figure 6 or Table 2.

### 3.2.1 Human Driver

A human-driven vehicle involves control on several levels. On the highest level, at each time instant the driver chooses a desired vehicle speed (which may be represented by $\omega_o^*$), the driver monitors the actual vehicle speed (which may be represented by $\omega_o$), and the driver issues an output torque request (which may be represented by $T_o^*$) intended to reduce the error between the desired and actual vehicle speeds. The driver's request $T_o^*$ is expressed by pressing the accelerator pedal (for positive acceleration) or the brake pedal (for negative acceleration). This request is sent on to the next lowest level, the power management unit.

### 3.2.2 Power Management Unit

The driver's request for an output torque at a given output speed amounts to an output power demand. The power management unit (PMU) is responsible for determining how this output power demand will be met by assigning a number of reference commands: $T_f^*$, the friction torque command; $T_e^*$, the engine torque command; $M^*$, the mode selection command; $T_c^*$, the control torque command; and $\omega_e^*$, the engine speed command. Assignment of these reference commands is made with the goal of meeting the driver's $T_o^*$ request in an efficient manner while maintaining battery state of charge within allowable limits. Note that the PMU is sometimes also known as the *Supervisory Controller*.

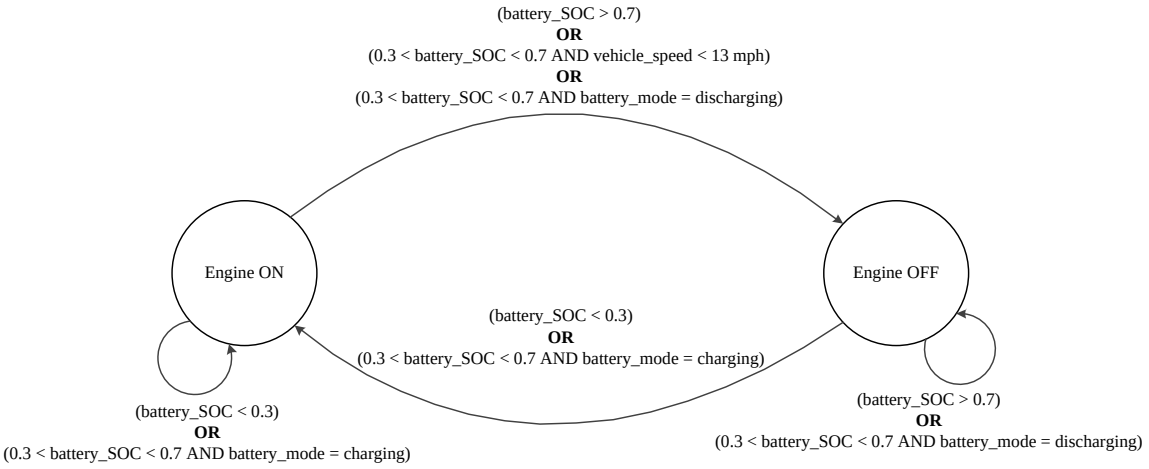


**Figure 7:** State transition diagram for power management.

To utilize the engine efficiently, its operation should be limited to one or more carefully chosen operating states identified by command values $(T_e^*, \omega_e^*)$. Besides operating the engine efficiently when it is on, the PMU also has the responsibility of turning the engine off at low and zero vehicle speeds $(T_e^* = 0, \omega_e^* = 0)$. Using the engine conservatively in this manner improves gas mileage, and also enables electronic assist and regenerative braking at low speeds. For the purposes of this study, it is assumed that the engine will be turned off for vehicle speeds below 13 mph. To maintain the health of the battery, the PMU is also responsible for maintaining the battery state of charge between 30% and 70%. The overall logic for charging and discharging the battery is kept simple on purpose since optimization of the PMU or supervisory controller is not the focus of this study. Figure 7 shows a state transition diagram illustrating the power management strategy used here.

The PMU also has the responsibility of determining the mode selection command, $M^*$ based on vehicle speed and engine speed. The logic behind this decision will be discussed in Section 3.2.4 on EVT Mode Shifting. As previously shown, the output torque is a weighted sum of three torques, $T_e$, $T_a$ and $T_b$, and the weights depend on the commanded mode $M^*$. Since engine torque has already been specified, the remaining two terms of the output torque must be used to control the transmission;

this control torque $T_c$ is defined by

$$T_c = \gamma_a T_a + \gamma_b T_b \tag{16}$$

and its reference command value is defined by

$$T_c^* = T_o^* - \gamma_e T_e^*. \tag{17}$$

The remaining reference command, $T_f^*$, comes into play when the transmission cannot produce a sufficiently large negative value of $T_c^*$; this issue is not specifically addressed in this study.

### 3.2.3 Transmission Control Unit

The next lowest level in control hierarchy is the transmission controller. It receives mode selection command $M^*$ as well as reference commands $(T_c^*, \omega_e^*)$, and it must determine corresponding reference commands $(T_a^*, T_b^*)$ for the motor-generator units in such a way that errors in control torque and engine speed will be kept small during transients and eliminated at steady state. This control design problem involves two inputs and two outputs, so there exists sufficient freedom to meet two regulation objectives simultaneously. The proposed solution is a multivariable type of state-feedback integral control; this solution has the advantage of not requiring any pre-assignment of specific control responsibilities for the two motor-generators units.

#### *3.2.3.1 Integral Control Structure*

The dynamic equations relating the actual outputs $(T_c, \omega_e)$ to the available inputs $(T_a^*, T_b^*)$ have been developed in previous chapter of this thesis. From those equations, combined with the integrated error equations shown below, it is possible to formulate and solve a linear quadratic regulator (LQR) problem to determine the feedback gain matrices that locate all eigenvalues of the overall system appropriately. Once gains have been determined, the resulting integral control structure may be expressed in

the form

$$\begin{bmatrix} u_a \\ u_b \end{bmatrix} = -K_1 \begin{bmatrix} \omega_e \\ \omega_o \end{bmatrix} - K_2 \begin{bmatrix} T_a \\ T_b \end{bmatrix} - K_3 \begin{bmatrix} \sigma_T \\ \sigma_\omega \end{bmatrix} \tag{18}$$

where the controller state variables are governed by

$$\begin{bmatrix} \dot{\sigma}_T \\ \dot{\sigma}_\omega \end{bmatrix} = \begin{bmatrix} T_c - T_c^* \\ \omega_e - \omega_e^* \end{bmatrix}. \tag{19}$$

The outputs of this structure $(u_a, u_b)$ are the tentative values for $(T_a^*, T_b^*)$, subject to limiting as appropriate. In actual practice, the speed feedback signals $(\omega_e, \omega_o)$ would most likely be obtained directly from rotational sensors, whereas the torque feedback signals $(T_a, T_b)$ would most likely be obtained indirectly from current sensors.

#### *3.2.3.2 Torque Command Limiting*

The motor-generator unit torque commands $(T_a^*, T_b^*)$ are generated from the outputs of the integral control structure $(u_a, u_b)$ according to

$$T_i^* = \begin{cases} U_i \text{sgn}\{u_i\} & \text{, if } |u_i| > U_i \\ u_i & \text{, otherwise} \end{cases}, \quad i = a, b$$

where the speed-dependent magnitude bounds are given by

$$U_i = \begin{cases} T_i^{\max} & \text{, if } |\omega_i| < P_i^{\max}/T_i^{\max} \\ 0 & \text{, if } |\omega_i| > \omega_i^{\max} \\ P_i^{\max}/|\omega_i| & \text{, otherwise} \end{cases}$$

so as to impose known constant-torque limits at lower speeds and known constant-power limits at higher speeds.

### 3.2.4 EVT Mode Shifting

When a shift between EVT modes is desired, it is generally preferred that there be no speed difference between the plates of clutches that require engaging or disengaging; such a shift is called a synchronous shift, and it has the advantage that no power is dissipated due to slipping of plates.

If a synchronous shift from EVT-1 to EVT-2 is desired, then $C_1$ is initially engaged and hence one side of $C_2$ is stationary and the other side of $C_2$ is rotating; therefore, a synchronous shift would require that the rotating side of $C_2$ be brought to zero speed or, equivalently, that $\omega_a \to 0$, which is achieved in EVT-1 if $\omega_e \to -(\gamma_{ao}/\gamma_{ae})_1 \omega_o$.

If a synchronous shift from EVT-2 to EVT-1 is desired, then $C_2$ is initially engaged and hence one side of $C_1$ is stationary and the other side of $C_1$ is rotating; therefore, a synchronous shift would require that the rotating side of $C_1$ be brought to zero speed or, equivalently, that $\omega_a \to 0$, which is achieved in EVT-2 if $\omega_e \to -(\gamma_{ao}/\gamma_{ae})_2 \omega_o$.

Each of the four kinematic parameters involved is unique; however, the two ratios of interest are identical, which implies that synchronous shifts between EVT modes in either direction are achieved by adopting the engine speed command value

$$\omega_e^* = \frac{(1-\rho_1)(1+\rho_2)}{\rho_2}\omega_o.$$

On the other hand, since the engine operating state is preferably pre-specified, synchronous shifts between EVT modes in either direction are preferably achieved at vehicle speed

$$\omega_o = \frac{\rho_2}{(1-\rho_1)(1+\rho_2)}\omega_e^*. \tag{20}$$

For the parameter values assumed in the simulation section, with an engine speed of 2000 rpm, the critical vehicle speed would be approximately 26 mph.

Now, note that since the transmission parameters for EVT-1 and EVT-2 are different, the feedback gain matrices shown in (18) will be different for each mode. This implies that at the instant of a mode shift, the control law governing the outputs $(u_a, u_b)$ will change entirely thus introducing a jump discontinuity in $(u_a, u_b)$. This issue is not entirely problematic because the motor-generator units are torque-controlled components and their torque can be changed almost instantaneously depending on the time constant for torque control. Hence, it is assumed here that mode shifts are instantaneous for the purposes of simulation.

# CHAPTER IV

# SIMULATION RESULTS

The physical system is modeled by six state variables, the transmission controller adds two state variables, and the driver adds one state variable; the overall system being simulated therefore has nine state variables. The assumed parameter values for the simulated vehicle are specified in Table 3. All Matlab code for generating the simulation results shown in this chapter is provided in Appendix B.

These simulation results consider just one set of simulation parameters and just one set of LQR design coefficients. By adjusting the LQR design coefficients, one can tune the aggressiveness of the controller's corrective actions. Although the same LQR design coefficients are used for EVT-1 and EVT-2, since the transmission parameters are different for both EVT modes, the gain values are different. Accordingly, the gain matrices for EVT-1 are

$$K_1 = \begin{bmatrix} 3.6109 & -0.0031 \\ 1.0263 & 0.0156 \end{bmatrix}, \; K_2 = \begin{bmatrix} 1.7968 & -0.1774 \\ -0.2554 & 2.1060 \end{bmatrix}, \; K_3 = \begin{bmatrix} 4.8856 & -1.0633 \\ 1.2760 & 5.8627 \end{bmatrix}$$

and the gain matrices for EVT-2 are

$$K_1 = \begin{bmatrix} -0.8593 & 0.0137 \\ 4.2528 & 0.0043 \end{bmatrix}, \; K_2 = \begin{bmatrix} 1.2678 & -0.1945 \\ -0.2801 & 1.7136 \end{bmatrix}, \; K_3 = \begin{bmatrix} -1.3096 & 4.8254 \\ 5.7905 & 1.5715 \end{bmatrix}.$$

The efficient operating point for the engine is chosen to be $T_e = 100$ Nm and $\omega_e = 2000$ rpm. Now, the following sections will present results for individual operation in the Electric-1, EVT-1 and EVT-2 modes, followed by EVT mode shifting and a simulation of the full UDDS drive cycle.

**Table 3:** Modeling Parameters

| Parameter | Value |
|---|---|
| $m_v$ | 1750 kg |
| $r_w$ | 0.35 m |
| $a_f$ | 2.64 $m^2$ |
| $c_d$ | 0.38 |
| $c_r$ | 0.007 |
| $\rho_f$ | 0.3 |
| $\rho_1$ | 44/104 |
| $\rho_2$ | 37/83 |
| $n_{p1i}$ | 27 |
| $n_{p1o}$ | 28 |
| $n_{p2}$ | 23 |
| $\omega_p^{\max}$ | 14000 rpm |
| $I_a$ | 0.08 kg $m^2$ |
| $I_b$ | 0.08 kg $m^2$ |
| $I_e$ | 0.18 kg $m^2$ |
| $I_o$ | 19.4 kg $m^2$ |
| $\tau_e$ | 200 ms |
| $P_a^{\max}$ | 50 kW |
| $T_a^{\max}$ | 200 Nm |
| $\omega_a^{\max}$ | 7500 rpm |
| $\tau_a$ | 200 ms |
| $\eta_a$ | 0.85 |
| $P_b^{\max}$ | 60 kW |
| $T_b^{\max}$ | 240 Nm |
| $\omega_b^{\max}$ | 9000 rpm |
| $\tau_b$ | 200 ms |
| $\eta_b$ | 0.85 |
| $V_s$ | 250 V |
| $Q_s$ | 40 Ah |
| $R_s$ | 90 m$\Omega$ |

## *4.1 Operation in Electric-1, EVT-1 and EVT-2*

Consider the first three minutes of the UDDS drive cycle, and assume that the PMU has commanded the TCU to operate in mode Electric-1. Figure 8 demonstrates that the driver goals are being met, Figure 9 demonstrates how the transmission controller is doing its job, and Figure 10 demonstrates the resulting battery power usage.

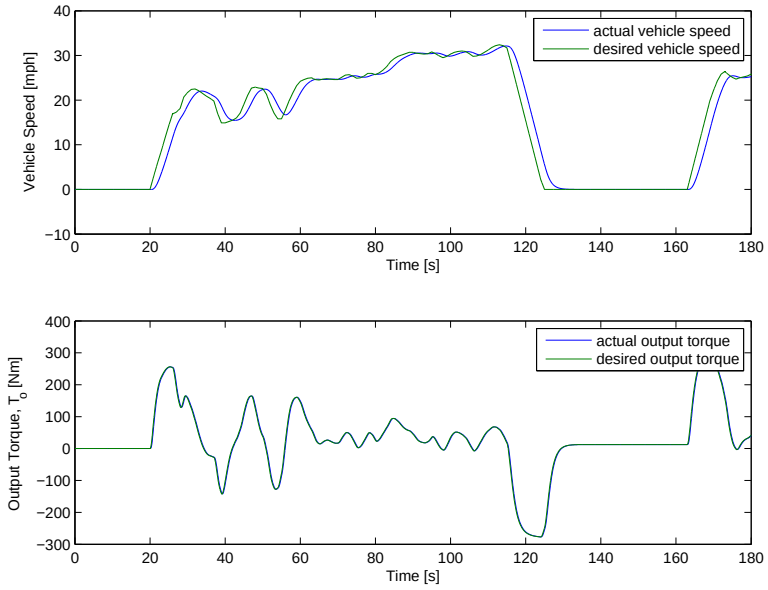


**Figure 8:** External response in Electric-1.

Recall that in mode Electric-1, the engine is turned off and the engine is supplying no power. Accordingly, battery power is 0 kW when the vehicle is at rest and the battery state of charge does not change. Also note that in Figure 10, when the vehicle is slowing down and braking power is being used, battery power is negative and state of charge increases. Having a negative battery power signifies that the battery is being charged and hence in this situation, regenerative braking is functioning as expected.

Consider again the first three minutes of the UDDS drive cycle, but assume that the PMU has commanded the TCU to operate in mode EVT-1 with $T_e = 100$ Nm and $\omega_e = 2000$ rpm. Figure 11 demonstrates that the driver goals are being met,

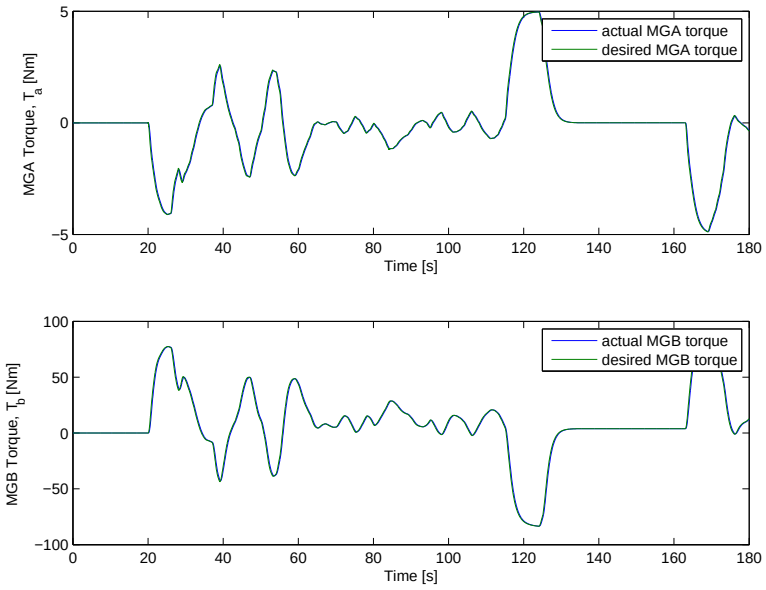


**Figure 9:** Transmission response in Electric-1.

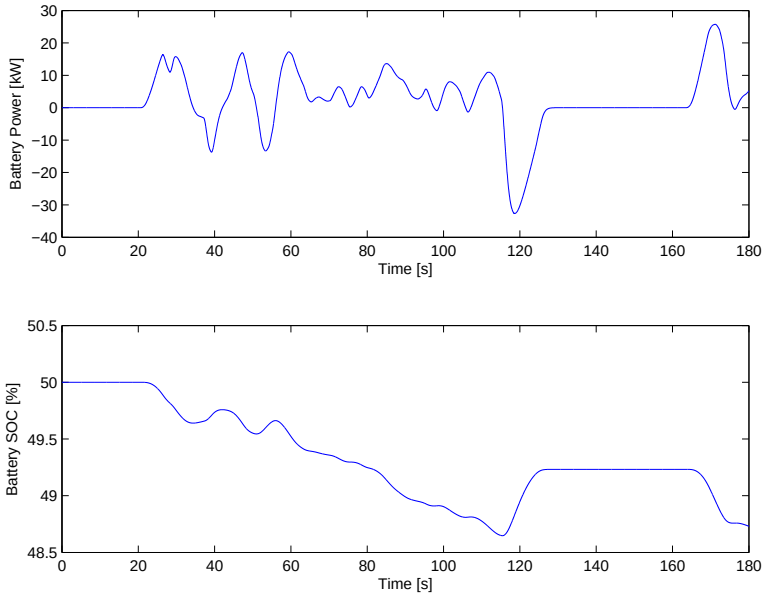


**Figure 10:** Battery usage in Electric-1.

Figure 12 demonstrates how the transmission controller is doing its job, and Figure 13 demonstrates the resulting battery power usage.

Note that even though the PMU described in Section 3.2.2 mentions that the engine will be turned off when the vehicle is at low speeds, this particular scenario

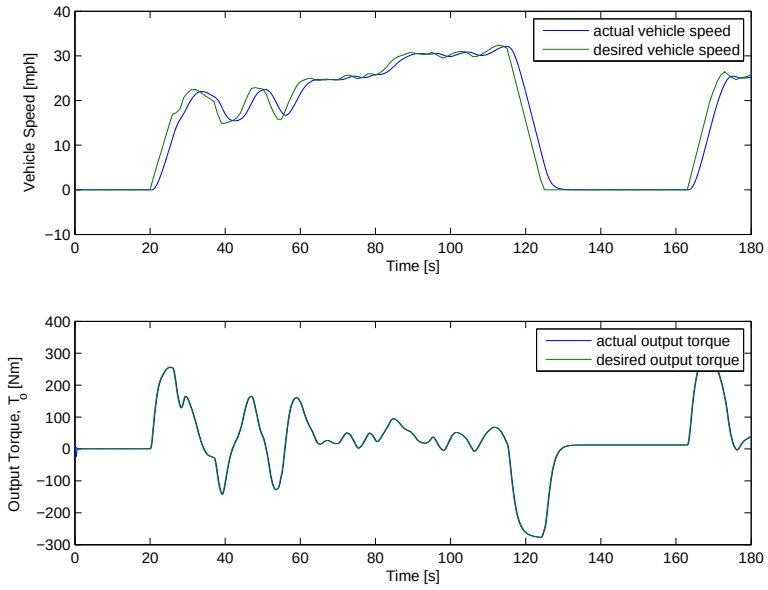


**Figure 11:** External response in EVT-1.

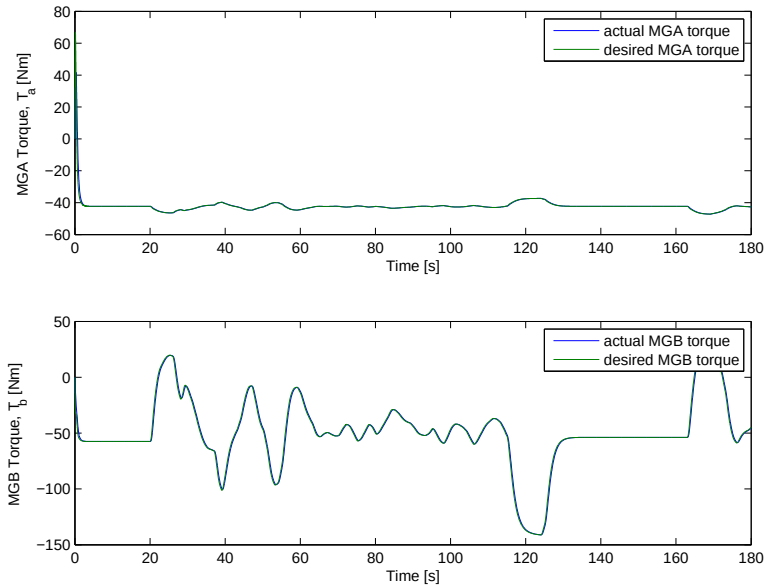


**Figure 12:** Transmission response in EVT-1.

assumes that the engine is on even if the vehicle is at rest. As a result of this assumption, note that in Figure 13, the battery power is negative i.e. the battery is getting charged even when the vehicle is at rest because the engine is on. Likewise, battery state of charge is constantly increasing because battery power is always negative in this scenario. Full functionality of the PMU as described in Section 3.2.2 will be

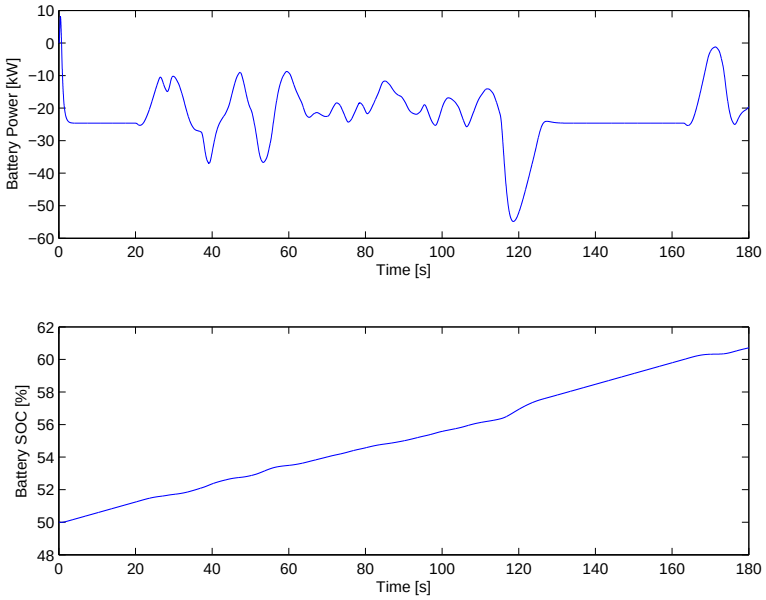


**Figure 13:** Battery usage in EVT-1.

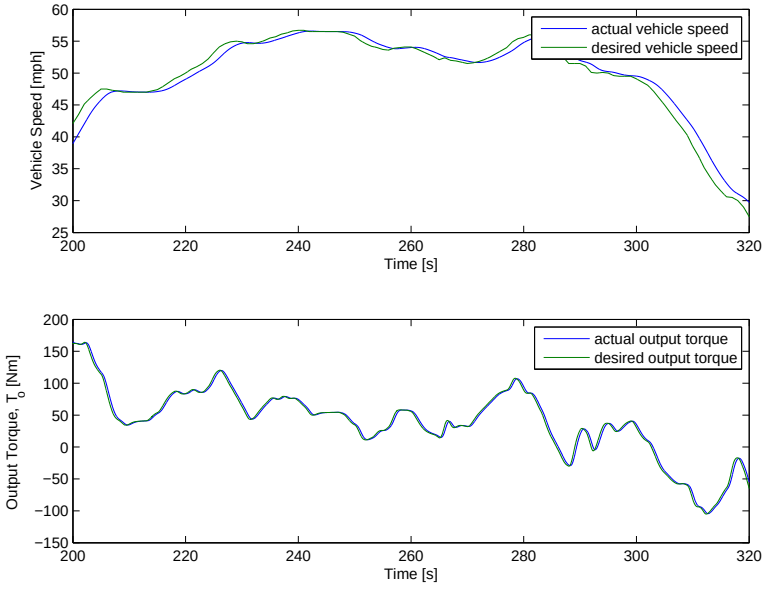


**Figure 14:** External response in EVT-2.

demonstrated in the full UDDS drive cycle simulation shown in Section 4.3.

Now consider a carefully chosen two minute interval of the UDDS drive cycle with high vehicle speeds, and assume that the PMU has commanded the TCU to operate in mode EVT-2 with $T_e = 100$ Nm and $\omega_e = 2000$ rpm. Recall that EVT-2 is feasible only for higher vehicle speeds (typically above 26 mph). Figure 14 demonstrates

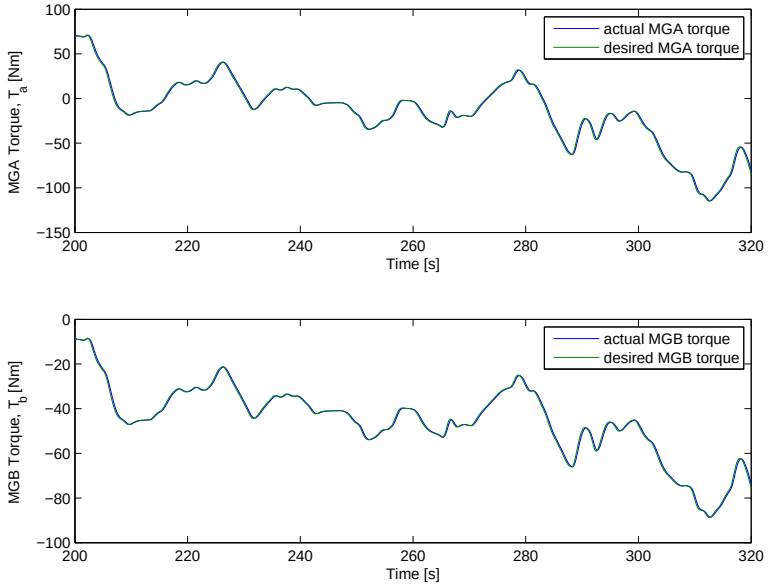


**Figure 15:** Transmission response in EVT-2.

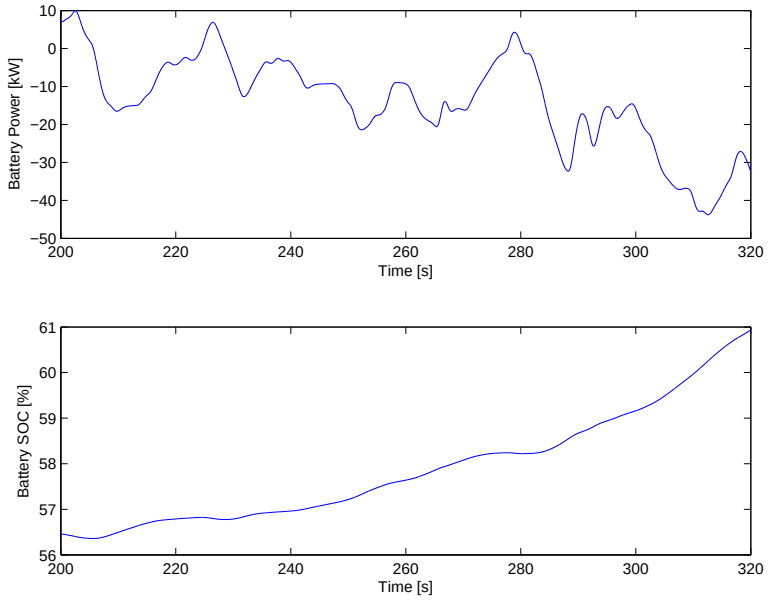


**Figure 16:** Battery usage in EVT-2.

that the driver goals are being met, Figure 15 demonstrates how the transmission controller is doing its job, and Figure 16 demonstrates the resulting battery power usage.

Both control objectives are met with the proposed control structure; the driver torque request is met and the engine speed is regulated. Therefore, the utility of the

proposed control structure for use in any one mode of operation has been demonstrated. What remains is to demonstrate successful shifting between modes; these results are shown in the next section.

## *4.2 EVT Mode Shifting Results*

Now that each operating mode has been tested and simulated individually, EVT mode shifting is achieved using the approach discussed in Section 3.2.4. Simulation results for an EVT-2 to EVT-1 mode shift from an interval of the UDDS drive cycle are presented below. Similar results can be produced for an EVT-1 to EVT-2 mode shift using the simulation code provided in Appendix B.

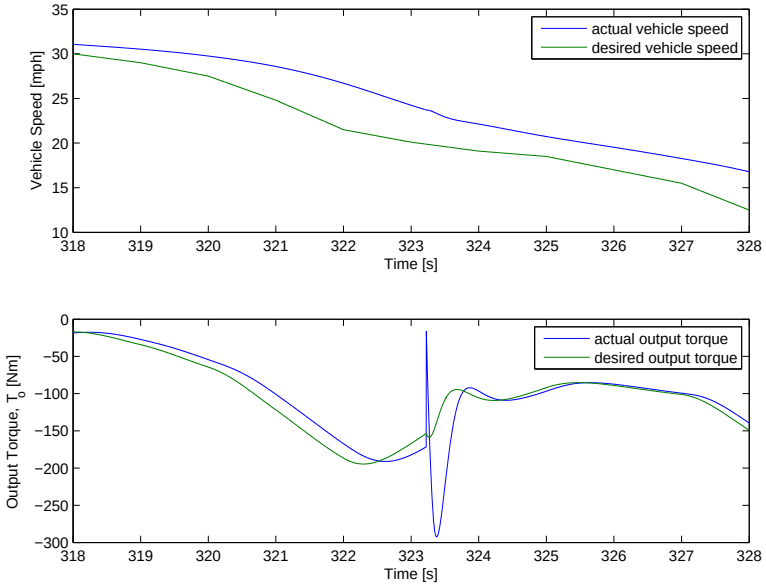


**Figure 17:** External response for EVT-2 to EVT-1 mode shift.

Assume that the PMU has commanded the TCU to operate with $T_e = 100$ Nm and $\omega_e = 2000$ rpm. The drive cycle simulation interval is chosen such that speed is gradually decreasing from 30 mph and the mode shift occurs at a critical mode shifting speed of 26 mph as mentioned in Section 3.2.4. Figure 17 demonstrates that the driver goals are being met, Figure 18 demonstrates the engine response to mode shift, Figure 19 demonstrates how the transmission controller is doing its job, and

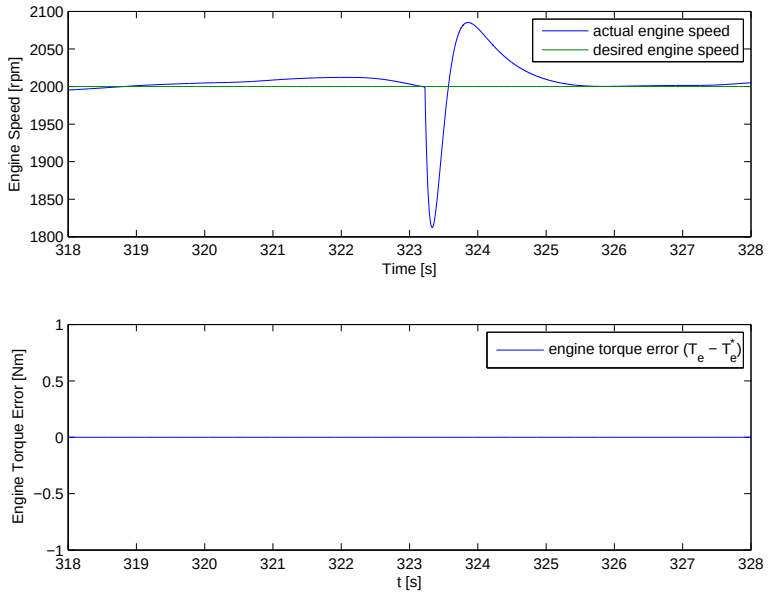


**Figure 18:** Engine response for EVT-2 to EVT-1 mode shift.

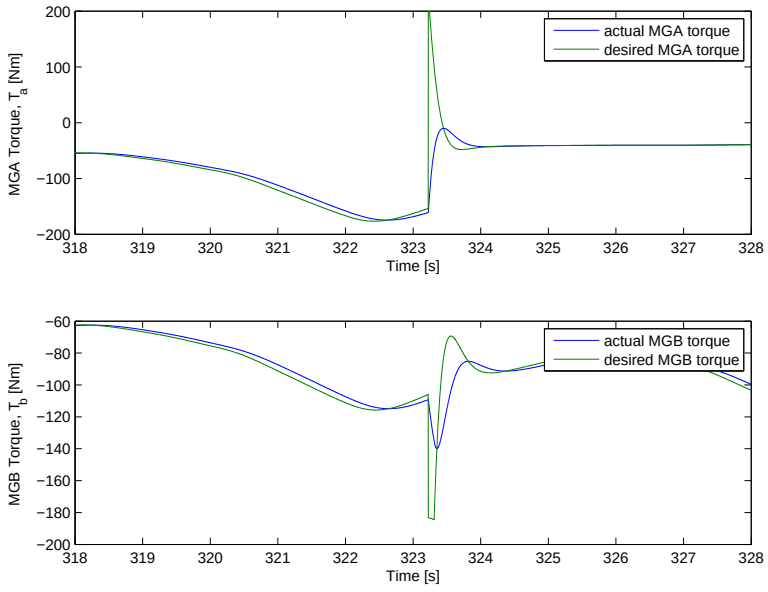


**Figure 19:** Transmission response for EVT-2 to EVT-1 mode shift.

Figure 20 demonstrates the resulting battery power usage.

Recall from (15) that output torque, $T_o$, is a weighted sum of $T_a$, $T_b$ and $T_e$ where each of the torques is a state variable of the system. Hence, one would expect $T_o$ to always be continuous and free from any jump discontinuities. However, $\gamma_a$, $\gamma_b$ and $\gamma_e$ from (15) are different for each EVT mode which explains the jump discontinuity

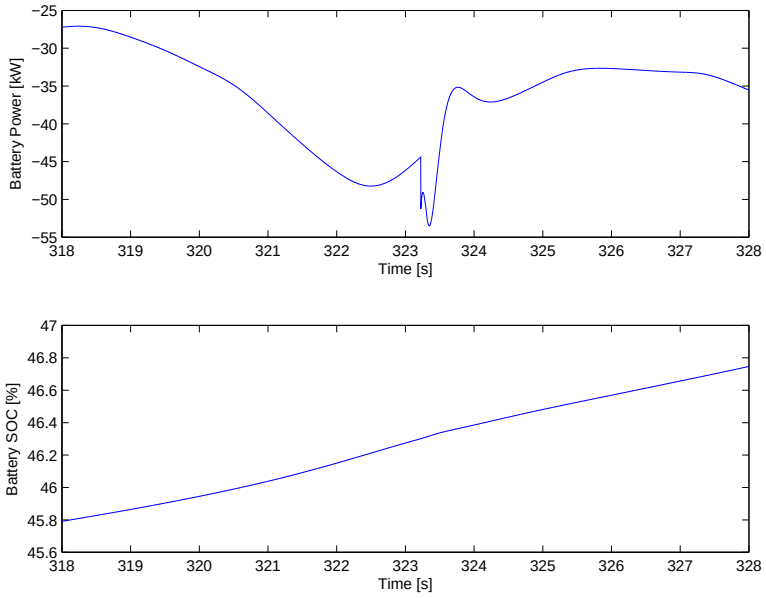


**Figure 20:** Battery usage for EVT-2 to EVT-1 mode shift.

in output torque at the instant of a mode shift as seen in Figure 17. Observe that, in Figure 18, the engine speed has a large transient at the instant of a mode shift. This is expected because the control law is changing and so are the electric machine torques that regulate engine speed to the desired operating point. Also observe that the transmission response or electric machine torques in Figure 19 have saturated reference torques to rapidly accommodate the change in dynamics of the transmission and control engine speed.

## *4.3 Full UDDS Drive Cycle Simulation*

In the previous sections, individual operating modes have been simulated and mode shifting has been tested for short intervals of the drive cycle. This section will focus on applying all features of the control system discussed in this thesis to a full UDDS drive cycle simulation. Once more, note that Figure 21 demonstrates that the driver goals are being met, Figure 23 demonstrates the engine response for the drive cycle, Figure 24 demonstrates how the transmission controller is doing its job, and Figure 25 demonstrates the resulting battery power usage for the entire drive cycle.

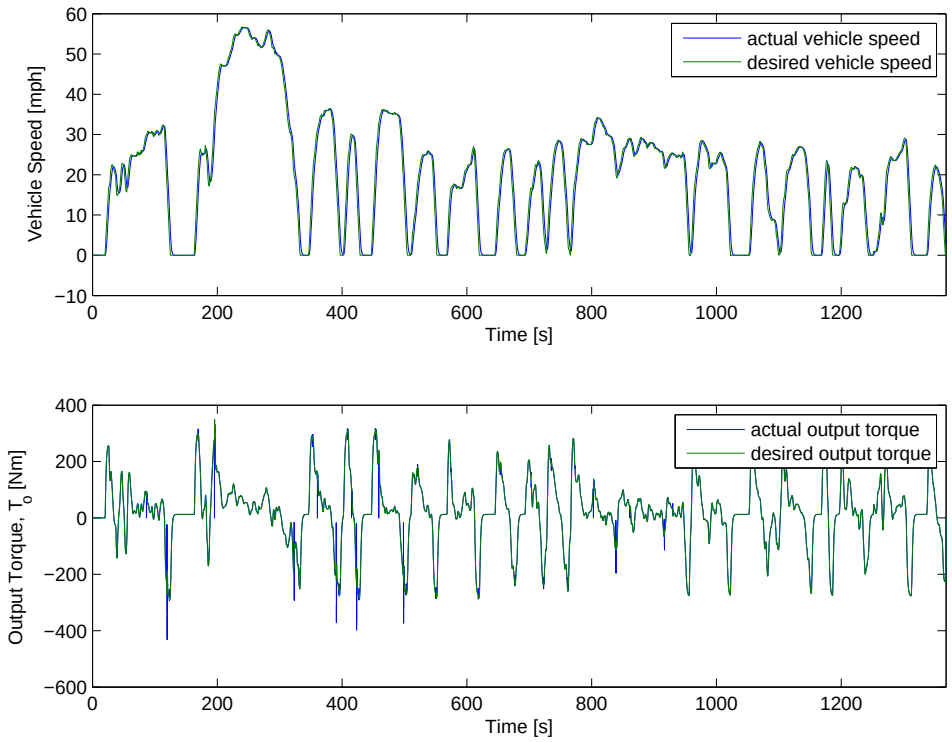


**Figure 21:** External response for UDDS drive cycle.

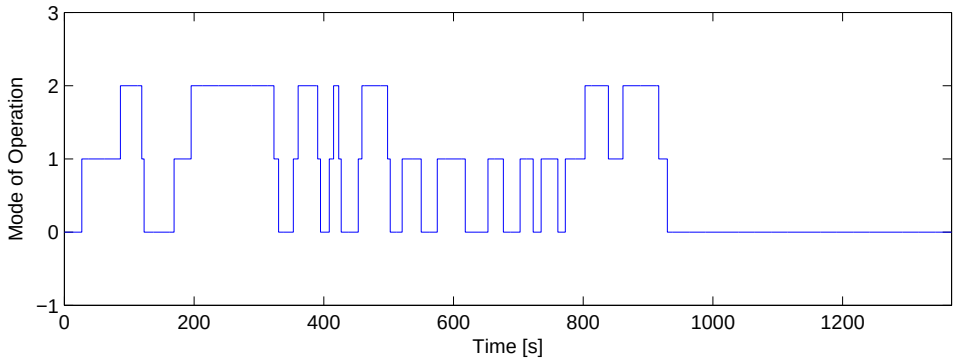


**Figure 22:** Operating modes for UDDS drive cycle.

Moreover, since there are multiple mode shifts throughout the drive cycle, Figure 22 illustrates the operating mode of the vehicle at each instant of time along the drive cycle. A value of 0 denotes that the operating mode is Electric-1, 1 denotes that the operating mode is EVT-1 and 2 denotes that the operating mode is EVT-2.

Observe that the PMU is exhibiting all features discussed in Section 3.2.2 and the accompanying state transition diagram in Figure 7. As seen in Figure 25, the

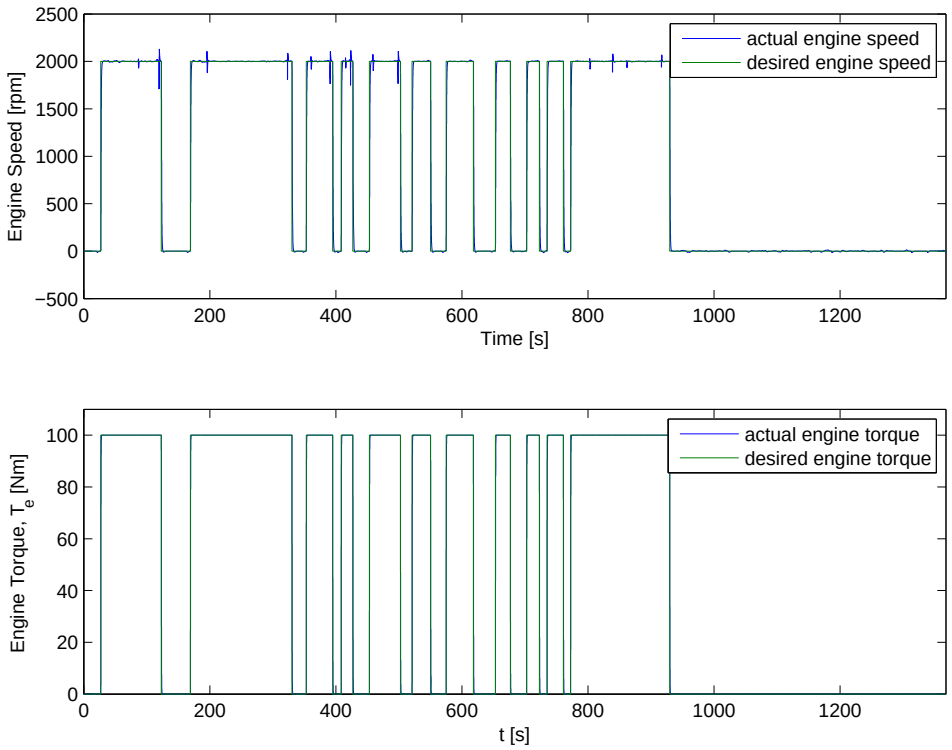


**Figure 23:** Engine response for UDDS drive cycle.

battery state of charge is being maintained between 30% and 70%. To achieve this goal, the engine was permanently turned off during the latter part of the drive cycle because battery state of charge had approached 70%. Turning off the engine allowed for expending some battery power while decreasing the state of charge. Also, observe in Figure 23 that the engine was regularly turned off at low vehicle speeds. Careful comparison of Figure 22 and Figure 23 will reveal that there are exactly 14 mode shifts between EVT-1 and EVT-2 throughout the drive cycle and there are 14 corresponding disturbances or *spikes* in engine speed during mode shift instances. Note that, in Figure 25, there are a few negative *spikes* in battery power because all braking power demand is being satisfied by the electric machines through regenerative braking.

Thus, with the proposed control structure, all control objectives of the PMU and TCU are met for the entire drive cycle; driver torque request is met, engine speed is regulated and battery state of charge is maintained within acceptable limits.

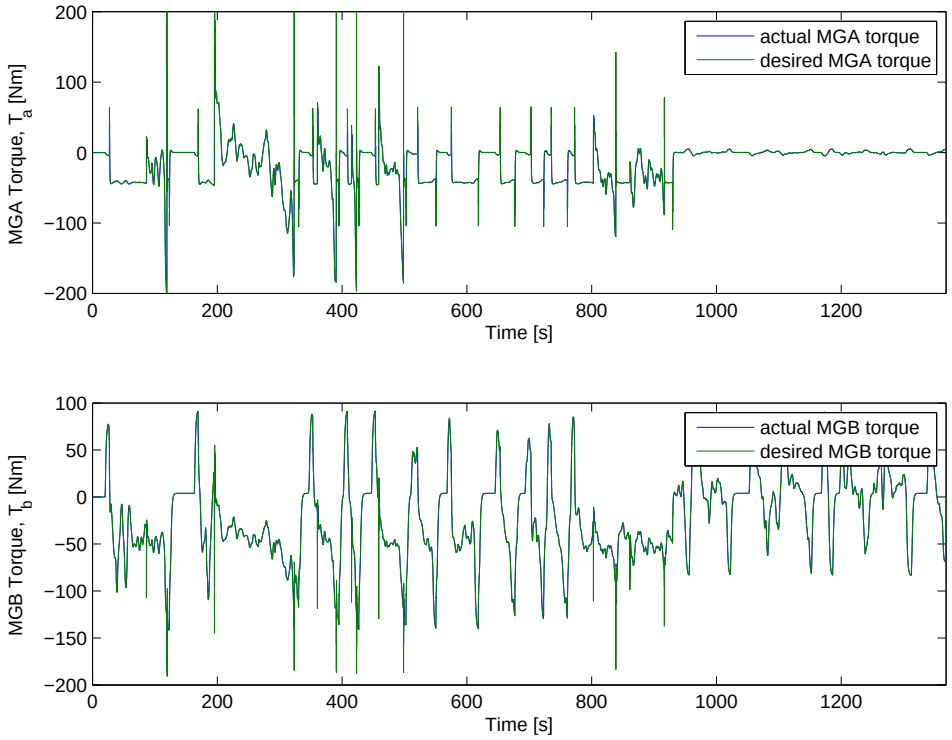


**Figure 24:** Transmission response for UDDS drive cycle.

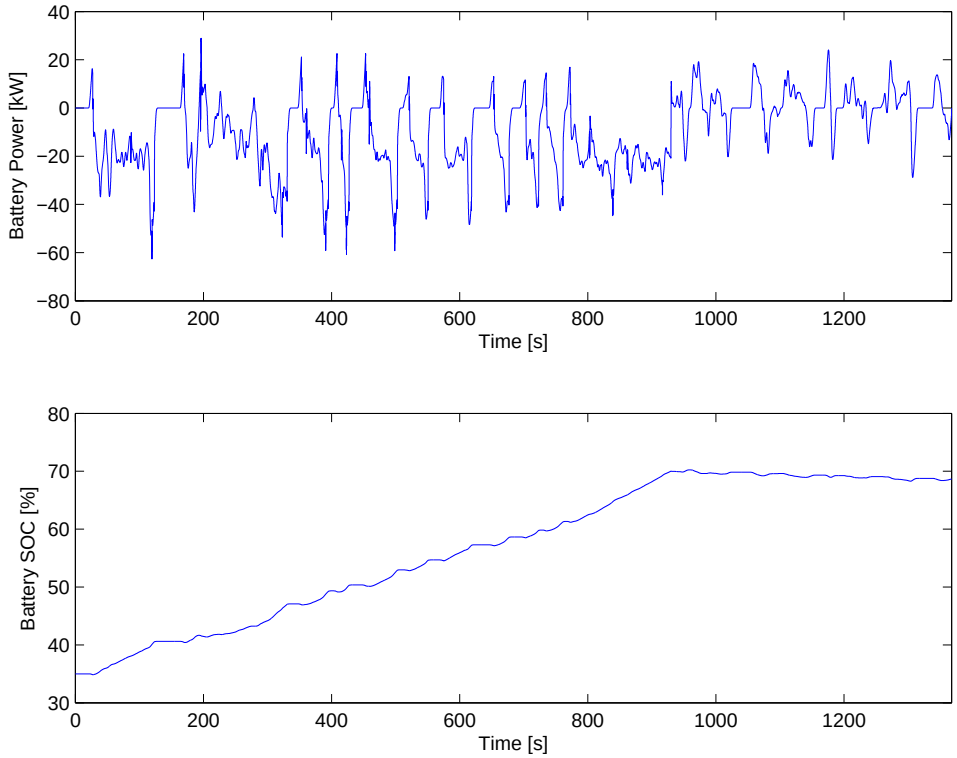


**Figure 25:** Battery usage for UDDS drive cycle.

# CHAPTER V

# CONCLUSION

## *5.1 Modeling and Control of Two-Mode EVT*

The objective of this thesis was to develop dynamic models for the two-mode FWD EVT, and to further develop a control system based on those models that is capable of meeting driver torque demands and performing synchronous mode shifts between different EVT modes while also accommodating preferred engine operating points. This thesis thus provides dynamic modeling details for a two-mode EVT. The mechanical subsystem consists of the planetary gear sets, the transmission and the engine whereas the electrical subsystem consists of the motor-generator units and battery pack. The dynamic equations for transmission dynamics are obtained using a power balance equation and kinematic constraints.

A clear definition of output torque using the derived dynamic model is provided. A comparison between the required output torque and available output torque in various operating modes at different vehicle speeds is also presented. This comparison clarifies whether or not a given powertrain design is capable of meeting desired performance requirements. The overall control system designed for the two-mode EVT is divided into multiple subsystems, including the human driver, the power management unit (PMU), the friction brakes, the combustion engine, the transmission control unit (TCU), and the motor-generator units. This thesis also describes a method for performing synchronous EVT mode shifts. The feedback gains for the transmission controller are determined using LQR optimization.

Simulation results for responses in individual operating modes, during EVT mode shifting, and for a full UDDS drive cycle are presented. Note the importance of

the full drive cycle simulation wherein all aspects of the overall designed control system including synchronous mode shifting, operation in multiple modes, power management, transmission control and human driver control are demonstrated. Thus, with the proposed control structure, all control objectives of the PMU and TCU are met for the entire drive cycle; the driver torque request is met, the engine speed is regulated and the battery state of charge is maintained within acceptable limits.

## *5.2 Future Work*

The control system designed in this thesis provides the design for usage of friction braking but uses regenerative braking for all its braking power in the simulations. However, in most vehicles, the motor-generator units may not be capable of providing all required braking power when the vehicle makes sudden stops. Hence, it will be important to implement friction brakes and divert some braking power demand to the friction brakes. This would avoid saturating the motor-generator units due to excessive torque demands from the TCU when the vehicle makes sudden stops.

The two-mode EVT is capable of operating in fixed gear modes. Future work will include implementing fixed gear modes and being able to perform mode shifts between fixed gear modes and EVT modes. Moreover, the logic for mode shifting can be improved by performing mode shifts within a pre-specified time interval of few seconds rather than assuming instantaneous mode shifts. Implementing gradual mode shifts will help eliminate step reference commands for electric machine torques. The PMU or supervisory controller implemented in this thesis is fairly basic and uses a simple algorithm for maintaining battery state of charge within acceptable limits. This PMU can be enhanced with a sophisticated power management strategy that uses optimization techniques while using the same TCU designed earlier. Note that the main focus of this thesis was to develop a transmission controller using general control theory concepts while developing a dynamic model for the transmission.

# APPENDIX A

## CODE FOR OUTPUT TORQUE CAPABILITY

```
clc, clear all, close all
global Ga Gb Ge Gao Gbo te

%% assumed conditions
EVT = 1;
we = 0;
te = 0;
% we = 2000*2*pi/60;
% te = 100;
drvcyc = 1;

%% model parameters
PaMax = 50e3;
TaMax = 200;
WaMax = 7500*2*pi/60;
PbMax = 60e3;
TbMax = 240;
WbMax = 9000*2*pi/60;

Rw = 0.35;
Gf = 0.3;

v = 0:80;
wo = v*0.44704/(Rw*Gf);

M = 1750;

C0 = 0.007*9.8*M;
C2 = 0.5*1.25*2.64*0.38;

Ie = 0.18;
Ia = 0.08;
Ib = 0.08;
Io = 0.1+M*(Gf*Rw)^2;

ns1 = 44;
nr1 = 104;
```

```
np1s = 27;
np1r = 28;
ns2 = 37;
nr2 = 83;
np2 = 23;
G1 = ns1/nr1;
G2 = ns2/nr2;

if EVT == 1
    Gae = 1/G1;
    Gao = -(1-G1)*(1+G2)/(G1*G2);
    Gbe = 0;
    Gbo = (1+G2)/G2;
end

if EVT == 2
    Gae = -G2/(1-G1-G1*G2);
    Gao = (1-G1)*(1+G2)/(1-G1-G1*G2);
    Gbe = 1/(1-G1-G1*G2);
    Gbo = -G1*(1+G2)/(1-G1-G1*G2);
end

Jee = Ie+Gae^2*Ia+Gbe^2*Ib;
Jeo = Gae*Gao*Ia+Gbe*Gbo*Ib;
Joo = Io+Gao^2*Ia+Gbo^2*Ib;

Jo = Joo-(Jeo/Jee)*Jeo;

Ga = Gao-(Jeo/Jee)*Gae;
Gb = Gbo-(Jeo/Jee)*Gbe;
Ge = -(Jeo/Jee);

%% inversion

data = load('udds.txt');
h = 0.1; %0.001;
t = 0:h:data(end,1);
woR = interp1(data(:,1),data(:,2),t)*0.44704/(Gf*Rw);

voR = zeros(1,length(t));
tlR = zeros(1,length(t));
toR = zeros(1,length(t));

for n = 1:length(t)-1
```

```
    voR(n) = Rw*Gf*woR(n);
    tlR(n) = Rw*Gf*(C0+C2*voR(n)^2)*sign(voR(n));
    toR(n) = tlR(n)+Jo*(woR(n+1)-woR(n))/h;

end

%% optimization
options=optimset('Algorithm','interior-point');

Ta_Max = NaN*zeros(1,length(wo));
Tb_Max = NaN*zeros(1,length(wo));
To_Max = NaN*zeros(1,length(wo));
Ta_Min = NaN*zeros(1,length(wo));
Tb_Min = NaN*zeros(1,length(wo));
To_Min = NaN*zeros(1,length(wo));
Ta_Max_ss = NaN*zeros(1,length(wo));
Tb_Max_ss = NaN*zeros(1,length(wo));
To_Max_ss = NaN*zeros(1,length(wo));
Ta_Min_ss = NaN*zeros(1,length(wo));
Tb_Min_ss = NaN*zeros(1,length(wo));
To_Min_ss = NaN*zeros(1,length(wo));

for n = 1:length(wo)

    w = [Gae Gao; Gbe Gbo]*[we;wo(n)];
    wa = w(1);
    wb = w(2);

    if abs(wa) < PaMax/TaMax
        Ua = TaMax;
    elseif abs(wa) > WaMax
        Ua = 0;
    else
        Ua = PaMax/abs(wa);
    end

    if abs(wb) < PbMax/TbMax
        Ub = TbMax;
    elseif abs(wb) > WbMax
        Ub = 0;
    else
        Ub = PbMax/abs(wb);
    end

    wp1s = ns1*(wb-wa)/np1s;
```

```
    wp1r = nr1*(we-wb)/np1r;
    wp2 = ns2*(wo-wb)/np2;

    if max([abs(wp1s),abs(wp1r),abs(wp2)]) < 14000*2*pi/60

        x0 = [0; 0];
        x = fmincon(@max_To,x0,[],[],[],[],[-Ua,-Ub],[Ua,Ub],[],...
            options);
        Ta_Max(n) = x(1);
        Tb_Max(n) = x(2);
        To_Max(n) = Ga*x(1)+Gb*x(2)+Ge*te;
        x = fmincon(@min_To,x0,[],[],[],[],[-Ua,-Ub],[Ua,Ub],[],...
            options);
        Ta_Min(n) = x(1);
        Tb_Min(n) = x(2);
        To_Min(n) = Ga*x(1)+Gb*x(2)+Ge*te;
        x = fmincon(@max_To_ss,x0,[],[],[],[],[-Ua,-Ub],[Ua,Ub],[],...
            options);
        Ta_Max_ss(n) = x(1);
        Tb_Max_ss(n) = x(2);
        To_Max_ss(n) = Gao*x(1)+Gbo*x(2);
        x = fmincon(@min_To_ss,x0,[],[],[],[],[-Ua,-Ub],[Ua,Ub],[],...
            options);
        Ta_Min_ss(n) = x(1);
        Tb_Min_ss(n) = x(2);
        To_Min_ss(n) = Gao*x(1)+Gbo*x(2);

    end

end

%% results
if drvcyc == 1
    figure
    subplot(211), plot(voR/0.44704,toR,'.r'), box on,
    hold on, plot(v,[To_Max;To_Min],'b','LineWidth',1.5), hold off
    xlabel('Vehicle Speed [mph]'), ylabel('Output Torque [Nm]'),
    axis([0 70 -1500 1500]), legend('UDDS Required Output Torque',...
        'Maximum Output Torque Available'),
    subplot(212), hold on, box on,
    h1 = plot(v,Ta_Max,'b','LineWidth',1.5);
    h2 = plot(v,Ta_Min,'b','LineWidth',1.5);
    h3 = plot(v,Tb_Max,'g','LineWidth',1.5);
    h4 = plot(v,Tb_Min,'g','LineWidth',1.5);
    hold off
```

```
    legend([h1 h3],{'Maximum MGA Torque','Maximum MGB Torque'})
    xlabel('Vehicle Speed [mph]'), ylabel('MGU Torque [Nm]'), ...
        axis([0 70 -300 300])
else
    figure, plot(v,To_Max,v,To_Min)
    figure, plot(v,Ta_Max,v,Ta_Min,v,Tb_Max,v,Tb_Min)
end

function f = max_To(x)
global Ga Gb Ge te

ta = x(1);
tb = x(2);

f = -(Ga*ta+Gb*tb+Ge*te);

function f = min_To(x)
global Ga Gb Ge te

ta = x(1);
tb = x(2);

f = Ga*ta+Gb*tb+Ge*te;

function f = max_To_ss(x)
global Gao Gbo

ta = x(1);
tb = x(2);

f = -(Gao*ta+Gbo*tb);

function f = min_To_ss(x)
global Gao Gbo

ta = x(1);
tb = x(2);

f = Gao*ta+Gbo*tb;
```

# APPENDIX B

## CODE FOR DRIVE CYCLE SIMULATIONS

```
ti = 0;
tf = 1369;

choice = menu('What would you like to simulate?',...
    'Full UDDS Drive Cycle','EVT-1 to EVT-2 Mode-Shifting',...
    'EVT-2 to EVT-1 Mode-Shifting');

if choice == 1
    % Full UDDS
    tiDisp = 0;
    tfDisp = 1368;
elseif choice == 2
    % EVT1 to EVT2 Mode-Shift
    tiDisp = 80;
    tfDisp = 95;
elseif choice == 3
    % EVT2 to EVT1 Mode-Shift
    tiDisp = 318;
    tfDisp = 328;
else
    % Full UDDS
    tiDisp = 0;
    tfDisp = 1368;
end

weON = 2000*2*pi/60;
teON = 100;
weOFF = 0;
teOFF = 0;

Vs = 250;               % OC voltage of battery
Qs = 40*60*60;          % ideal charge capacity
Rs = 0.09;              % internal resistance

Te = 0.2;               % time-constant for engine
Ta = 0.2;               % time-constant for MGA
Tb = 0.2;               % time-constant for MGB
```

```
PaMax = 50e3;           % max power for MGA
TaMax = 200;            % max torque for MGA
WaMax = 7500*2*pi/60;   % max speed for MGA
PbMax = 60e3;           % max power for MGB
TbMax = 240;            % max torque for MGB
WbMax = 9000*2*pi/60;   % max speed for MGB

M = 1750;               % mass of vehicle
Cr = 0.007;             % rolling resistance coefficient
g = 9.8;                % acceleration due to gravity
Af = 2.64;              % frontal area
Cd = 0.38;              % aerodynamic drag coefficient
Ra = 1.25;              % density of air
Rw = 0.35;              % wheel radius
Gf = 0.3;               % final drive ratio

C0 = Cr*g*M;
C2 = 0.5*Ra*Af*Cd;

Ie = 0.18;              % engine inertia
Ia = 0.08;              % MGA inertia
Ib = 0.08;              % MGB inertia
Io = 0.1+M*(Gf*Rw)^2;   % output shaft inertia

G1 = 44/104;            % ratio for PG1
G2 = 37/83;             % ratio for PG2

Gae_EVT1 = 1/G1;
Gao_EVT1 = -(1-G1)*(1+G2)/(G1*G2);
Gbe_EVT1 = 0;
Gbo_EVT1 = (1+G2)/G2;
G_EVT1 = [Gae_EVT1 Gao_EVT1; Gbe_EVT1 Gbo_EVT1];

Gae_EVT2 = -G2/(1-G1-G1*G2);
Gao_EVT2 = (1-G1)*(1+G2)/(1-G1-G1*G2);
Gbe_EVT2 = 1/(1-G1-G1*G2);
Gbo_EVT2 = -G1*(1+G2)/(1-G1-G1*G2);
G_EVT2 = [Gae_EVT2 Gao_EVT2; Gbe_EVT2 Gbo_EVT2];

Jee_EVT1 = Ie+Gae_EVT1^2*Ia+Gbe_EVT1^2*Ib;
Joo_EVT1 = Io+Gao_EVT1^2*Ia+Gbo_EVT1^2*Ib;
Jeo_EVT1 = Gae_EVT1*Gao_EVT1*Ia+Gbe_EVT1*Gbo_EVT1*Ib;
J_EVT1 = [Jee_EVT1 Jeo_EVT1; Jeo_EVT1 Joo_EVT1];
invJ_EVT1 = J_EVT1\eye(2);
```

```
Jee_EVT2 = Ie+Gae_EVT2^2*Ia+Gbe_EVT2^2*Ib;
Joo_EVT2 = Io+Gao_EVT2^2*Ia+Gbo_EVT2^2*Ib;
Jeo_EVT2 = Gae_EVT2*Gao_EVT2*Ia+Gbe_EVT2*Gbo_EVT2*Ib;
J_EVT2 = [Jee_EVT2 Jeo_EVT2; Jeo_EVT2 Joo_EVT2];
invJ_EVT2 = J_EVT2\eye(2);

Ga_EVT1 = Gao_EVT1-(Jeo_EVT1/Jee_EVT1)*Gae_EVT1;
Gb_EVT1 = Gbo_EVT1-(Jeo_EVT1/Jee_EVT1)*Gbe_EVT1;
Ge_EVT1 = -(Jeo_EVT1/Jee_EVT1);

Ga_EVT2 = Gao_EVT2-(Jeo_EVT2/Jee_EVT2)*Gae_EVT2;
Gb_EVT2 = Gbo_EVT2-(Jeo_EVT2/Jee_EVT2)*Gbe_EVT2;
Ge_EVT2 = -(Jeo_EVT2/Jee_EVT2);

K1d = 38;
K2d = 19;

mph = 1;
mph2mps = 0.44704;
alpha = Ra*Af*Cd*(Gf*Rw)^3*(mph*mph2mps/(Gf*Rw));

A11_EVT1 = invJ_EVT1*diag([0,-alpha]);
A12_EVT1 = invJ_EVT1*G_EVT1';
A21_EVT1 = zeros(2,2);
A22_EVT1 = [-1/Ta 0; 0 -1/Tb];
A_EVT1 = [A11_EVT1 A12_EVT1; A21_EVT1 A22_EVT1];

B1_EVT1 = zeros(2,2);
B2_EVT1 = [1/Ta 0; 0 1/Tb];
B_EVT1 = [B1_EVT1; B2_EVT1];

C_EVT1 = [ 1 0 0 0; 0 0 Ga_EVT1 Gb_EVT1];

AA_EVT1 = [A_EVT1 zeros(4,2); C_EVT1 zeros(2,2)];
BB_EVT1 = [B_EVT1; zeros(2,2)];
CC_EVT1 = [C_EVT1; 0 0 1 0; 0 0 0 1];

A11_EVT2 = invJ_EVT2*diag([0,-alpha]);
A12_EVT2 = invJ_EVT2*G_EVT2';
A21_EVT2 = zeros(2,2);
A22_EVT2 = [-1/Ta 0; 0 -1/Tb];
A_EVT2 = [A11_EVT2 A12_EVT2; A21_EVT2 A22_EVT2];

B1_EVT2 = zeros(2,2);
B2_EVT2 = [1/Ta 0; 0 1/Tb];
```

```
B_EVT2 = [B1_EVT2; B2_EVT2];

C_EVT2 = [ 1 0 0 0; 0 0 Ga_EVT2 Gb_EVT2];

AA_EVT2 = [A_EVT2 zeros(4,2); C_EVT2 zeros(2,2)];
BB_EVT2 = [B_EVT2; zeros(2,2)];
CC_EVT2 = [C_EVT2; 0 0 1 0; 0 0 0 1];

QQ = diag([1/20^2,1/30^2,1/50^2,1/60^2,1/10^2,1/10^2]);
RR = diag([1/50^2,1/60^2]);

KK_EVT1 = lqr(AA_EVT1,BB_EVT1,QQ,RR);
K1_EVT1 = KK_EVT1(1:2,1:2);
K2_EVT1 = KK_EVT1(1:2,3:4);
K3_EVT1 = KK_EVT1(1:2,5:6);

KK_EVT2 = lqr(AA_EVT2,BB_EVT2,QQ,RR);
K1_EVT2 = KK_EVT2(1:2,1:2);
K2_EVT2 = KK_EVT2(1:2,3:4);
K3_EVT2 = KK_EVT2(1:2,5:6);

woShift = (G2/((1-G1)*(1+G2)))*weON;
wHysShift = 11;
woUP = woShift + wHysShift;
woDOWN = woShift - wHysShift;

woENG = 13*mph2mps/(Gf*Rw);
wHysENG = 5;
woENGON = woENG + wHysENG;
woENGOFF = woENG - wHysENG;
weRdefault = weOFF;
teRdefault = teOFF;

data = load('udds.txt');
h = 0.001;
t = ti:h:data(tf,1);
woR = interp1(data(:,1),data(:,2),t)*mph2mps/(Gf*Rw);

we = zeros(1,length(t));
wo = zeros(1,length(t));
qs = zeros(1,length(t));
te = zeros(1,length(t));
ta = zeros(1,length(t));
tb = zeros(1,length(t));
sd = zeros(1,length(t));
```

```
sw = zeros(1,length(t));
st = zeros(1,length(t));

wa = zeros(1,length(t));
wb = zeros(1,length(t));
pl = zeros(1,length(t));
tl = zeros(1,length(t));
tc = zeros(1,length(t));
to = zeros(1,length(t));
mode = zeros(1,length(t));

weR = zeros(1,length(t));
teR = zeros(1,length(t));
toR = zeros(1,length(t));
tcR = zeros(1,length(t));
taR = zeros(1,length(t));
tbR = zeros(1,length(t));

qs(1) = 0.35;
EVT = 1;
battMode = 1;

for n = 1:length(t)-1

    % Supervisory control
    if wo(n) <= woDOWN
        EVT = 1;
        mode(n) = 1;
    elseif wo(n) >= woUP
        EVT = 2;
        mode(n) = 2;
    else
        if n ~= 1
            mode(n) = abs(mode(n-1));
        else
            error('mode vector is not being populated')
        end
    end

    if qs(n) >= 0.7
        weRdefault = weOFF;
        teRdefault = teOFF;
        battMode = 0;               % discharge battery
    elseif qs(n) <= 0.3
        weRdefault = weON;
```

```
    teRdefault = teON;
    battMode = 1;               % charge battery
else
    if battMode == 1
        if wo(n) >= woENGON
            weRdefault = weON;
            teRdefault = teON;
        elseif wo(n) <= woENGOFF
            weRdefault = weOFF;
            teRdefault = teOFF;
        end
    elseif battMode == 0
        weRdefault = weOFF;
        teRdefault = teOFF;
    end
end

weR(n) = weRdefault;
teR(n) = teRdefault;

if (weRdefault == weOFF) && (mode(n) == 1)
    mode(n) = -1;
elseif (weRdefault == weOFF) && (mode(n) == 2)
    mode(n) = -2;
end

v = Rw*Gf*wo(n);
tl(n) = Rw*Gf*(C0+C2*v^2)*sign(v);

if EVT == 1
    w = G_EVT1*[we(n);wo(n)];
    tc(n) = Ga_EVT1*ta(n)+Gb_EVT1*tb(n);
    to(n) = tc(n)+Ge_EVT1*te(n);
    toR(n) = -K1d*wo(n)-K2d*sd(n);
    tcR(n) = toR(n)-Ge_EVT1*teR(n);
    u = -K1_EVT1*[we(n);wo(n)]-K2_EVT1*[ta(n);tb(n)]...
        -K3_EVT1*[sw(n);st(n)];
    x = [we(n);wo(n)]+h*invJ_EVT1*(G_EVT1'*[ta(n);tb(n)]...
        +[te(n);-tl(n)]);
elseif EVT == 2
    w = G_EVT2*[we(n);wo(n)];
    tc(n) = Ga_EVT2*ta(n)+Gb_EVT2*tb(n);
    to(n) = tc(n)+Ge_EVT2*te(n);
    toR(n) = -K1d*wo(n)-K2d*sd(n);
    tcR(n) = toR(n)-Ge_EVT2*teR(n);
```

```
    u = -K1_EVT2*[we(n);wo(n)]-K2_EVT2*[ta(n);tb(n)]...
        -K3_EVT2*[sw(n);st(n)];
    x = [we(n);wo(n)]+h*invJ_EVT2*(G_EVT2'*[ta(n);tb(n)]...
        +[te(n);-tl(n)]);
end
wa(n) = w(1);
wb(n) = w(2);
pl(n) = (ta(n)*wa(n)+tb(n)*wb(n))/0.85;

if abs(wa(n)) < PaMax/TaMax
    Ua = TaMax;
elseif abs(wa(n)) > WaMax
    Ua = 0;
else
    Ua = PaMax/abs(wa(n));
end
if abs(wb(n)) < PbMax/TbMax
    Ub = TbMax;
elseif abs(wb(n)) > WbMax
    Ub = 0;
else
    Ub = PbMax/abs(wb(n));
end
if abs(u(1)) > Ua
    taR(n) = Ua*sign(u(1));
else
    taR(n) = u(1);
end
if abs(u(2)) > Ub
    tbR(n) = Ub*sign(u(2));
else
    tbR(n) = u(2);
end

we(n+1) = x(1);
wo(n+1) = x(2);

qs(n+1) = qs(n)-h*((Vs-sqrt(Vs^2-4*Rs*pl(n)))/(2*Rs*Qs));

te(n+1) = te(n)-h*((te(n)-teR(n))/Te);
ta(n+1) = ta(n)-h*((ta(n)-taR(n))/Ta);
tb(n+1) = tb(n)-h*((tb(n)-tbR(n))/Tb);

sd(n+1) = sd(n)+h*(wo(n)-woR(n));
sw(n+1) = sw(n)+h*(we(n)-weR(n));
```

```
    st(n+1) = st(n)+h*(tc(n)-tcR(n));

end

%% Plot figure - add final data points
figure
subplot(211), plot(t,we*60/(2*pi),t,weR*60/(2*pi)), box on,
ylabel('Engine Speed [rpm]'), xlabel('Time [s]'), xlim([tiDisp tfDisp]),
legend('actual engine speed','desired engine speed');
subplot(212), plot(t,te,t,teR), xlim([tiDisp tfDisp]), ylim([0 110]),
ylabel('Engine Torque, T_e [Nm]'), xlabel('t [s]'),
box on, legend('actual engine torque','desired engine torque');

figure
subplot(211), plot(t,wo*(Gf*Rw)/mph2mps,t,woR*(Gf*Rw)/mph2mps),
ylabel('Vehicle Speed [mph]'), xlabel('Time [s]'), xlim([tiDisp tfDisp]),
box on, legend('actual vehicle speed','desired vehicle speed');
subplot(212), plot(t,to,t,toR), xlim([tiDisp tfDisp]), box on,
ylabel('Output Torque, T_o [Nm]'), xlabel('Time [s]'),
legend('actual output torque','desired output torque');

figure
subplot(211), plot(t,ta,t,taR), xlim([tiDisp tfDisp]), box on,
ylabel('MGA Torque, T_a [Nm]'), xlabel('Time [s]'),
legend('actual MGA torque','desired MGA torque');
subplot(212), plot(t,tb,t,tbR), xlim([tiDisp tfDisp]), box on,
ylabel('MGB Torque, T_b [Nm]'), xlabel('Time [s]'),
legend('actual MGB torque','desired MGB torque');

figure
subplot(211), plot(t,pl/1000), xlim([tiDisp tfDisp]), box on,
ylabel('Battery Power [kW]'), xlabel('Time [s]');
subplot(212), plot(t,qs*100), xlim([tiDisp tfDisp]), box on,
ylabel('Battery SOC [%]'), xlabel('Time [s]');

mode(mode==-1) = 0;
figure
subplot(211), plot(t,mode), xlim([tiDisp tfDisp]), ylim([-1 3]),
ylabel('Mode of Operation'), xlabel('Time [s]');
```

# REFERENCES


[1] J. Liu and H. Peng, "Modeling and Control of a Power-Split Hybrid Vehicle," *IEEE Transactions on Control Systems Technology*, vol. 16, no. 6, pp. 1242–1251, 2008.

[2] J. Kim, N. Kim, S. Hwang, Y. Hori and H. Kim, "Motor Control of Input-Split Hybrid Electric Vehicles," *International Journal of Automotive Technology*, vol. 10, no. 6, pp. 733–742, 2009.

[3] T. Grewe, B. Conlon and A. Holmes, "Defining the General Motors Two-Mode Hybrid Transmission," SAE Paper 2007-01-0273.

[4] J. Hendrickson, A. Holmes and D. Freiman, "General Motors Front Wheel Drive Two-Mode Hybrid Transmission," SAE Paper 2009-01-0508.

[5] J. Kim, T. Kim, B. Min, S. Hwang and H. Kim, "Mode Control Strategy for a Two-Mode Hybrid Electric Vehicle Using Electrically Variable Transmission (EVT) and Fixed-Gear Mode," *IEEE Transactions on Vehicular Technology*, vol. 60, no. 3, pp. 793–803, 2011.

[6] N. Kim, J. Kim and H. Kim, "Control Strategy for a Dual-Mode Electromechanical, Infinitely Variable Transmission for Hybrid Electric Vehicles," *Proc. Inst. Mech. Eng. D: J. Automobile Eng.*, vol. 222, no. 9, pp. 1587–1601, 2008.

[7] T. M. Steinmetz, A. H. Heap, G. A. Hubbard and J. F. Sah, "Speed Control for an Electrically Variable Transmission," US Patent 7,219,000, 2007.

[8] F. Syed, M. Kuang, J. Czubay and H. Ying, "Derivation and Experimental Validation of a Power-Split Hybrid Electric Vehicle Model," *IEEE Transactions on Vehicular Technology*, vol. 55, no. 6, pp. 1731–1747, 2006.

[9] J. Arata, M. Leamy, J. Meisel, K. Cunefare and D. Taylor, "Backward-Looking Simulation of the Toyota Prius and General Motors Two-Mode Power-Split HEV Powertrains," SAE Paper 2011-01-0948.

[10] J. Meisel, "Kinematic Study of the GM Front-Wheel Drive Two-Mode Transmission and the Toyota Hybrid System THS-II Transmission," SAE Paper 2011-01-0876.

[11] J. Wishart, Y. Zhou, Z. Dong and F. Firmani, "Dynamic Modeling and Simulation of a Multi-Regime Hybrid Vehicle Powertrain Architecture," *International Journal of Electric and Hybrid Vehicles*, vol. 1, no. 2, pp. 188–219, 2008.

[12] F. Syed, M. Kuang, M. Smith, S. Okubo and H. Ying, "Fuzzy Gain-Scheduling Proportional-Integral Control for Improving Engine Power and Speed Behavior in a Hybrid Electric Vehicle," *IEEE Transactions on Vehicular Technology*, vol. 58, no. 1, pp. 69–84, 2009.

[13] K. Patil, T. Maxwell, S. Bayne and R. Gale, "Vehicle Development Process for EcoCAR: The Next Challenge Competition," *2010 IEEE Vehicle Power and Propulsion Conference (VPPC)*, 2010.

[14] J. D. Wishart, Y. Zhou and Z. Dong, "Review, Modelling and Simulation of Two-Mode Hybrid Vehicle Architecture," *Proc. ASME Int. Des. Eng. Tech. Conf. Comput. Inf. Eng. Conf.*, Las Vegas, NV, 2007.

[15] K. Wipke, M. Cuddy and S. Burch, "ADVISOR 2.1: A User-Friendly Advanced Powertrain Simulation Using a Combined Backward/Forward Approach," *IEEE Transactions on Vehicular Technology*, vol. 48, no. 6, pp. 1751–1761, 1999.

[16] D. G. Taylor, A. S. Katariya, "Dynamic Modeling and Feedback Control of a Two-Mode Electrically Variable Transmission," *2012 IEEE International Electric Vehicle Conference (IEVC)*, pp. 1–7, 2012.